

1 **Evaluation of shallow landslide triggering scenarios**  
2 **through a physically-based approach: an example of**  
3 **application in the southern Messina area (north-eastern**  
4 **Sicily, Italy)**

5  
6 **L. Schilirò<sup>1</sup>, C. Esposito<sup>1</sup>, G. Scarascia Mugnozza<sup>1</sup>**

7  
8 [1]{Department of Earth Sciences, “Sapienza” University of Rome, Rome, Italy}

9 Correspondence to: L. Schilirò (luca.schiliro@uniroma1.it)

10  
11 **Abstract**

12 Rainfall-induced shallow landslides are a widespread phenomenon that frequently causes  
13 substantial damage to property, as well as numerous casualties. In recent years a wide range  
14 of physically-based models has been developed to analyze the triggering process of these  
15 events. Specifically, in this paper we propose an approach for the evaluation of different  
16 shallow landslide triggering scenarios by means of TRIGRS numerical model. For the  
17 validation of the model, a back-analysis of the landslide event occurred in the study area  
18 (located SW of Messina, north-eastern Sicily, Italy) on 1 October 2009 was performed, by  
19 using different methods and techniques for the definition of the input parameters. After  
20 evaluating the reliability of the model through the comparison with the 2009 landslide  
21 inventory, different triggering scenarios were defined using rainfall values derived from the  
22 rainfall probability curves, reconstructed on the basis of daily and hourly historical rainfall  
23 data. The results emphasize how these phenomena are likely to occur in the area, given that  
24 even short-duration (1-3 hours) rainfall events having a relatively low return period (e.g. 10-20  
25 years) can trigger numerous slope failures. On the contrary, for the same rainfall amount, the  
26 daily simulations underestimate the instability conditions. The high susceptibility to shallow  
27 landslides in this area is testified by the high number of landslide/flood events occurred in the  
28 past and summarized in this paper by means of archival researches. Considering the main

1 features of the proposed approach, the authors suggest that this methodology could be applied  
2 to different areas, even for the development of landslide early warning systems.

## 4 **1 Introduction**

5 Landslides triggered by rainstorms occur in many part of the world and cause significant  
6 damage and loss to affected people, organizations and institutions as well as to the  
7 environment (Glade, 1997; Nadim et al., 2006; Petley, 2012). Within this category of natural  
8 disasters, shallow landslides (in particular debris-flows) pose a serious threat to life or  
9 property, in particular due to their high velocity, impact forces and long runout, combined  
10 with poor temporal predictability (Jacob and Hungr, 2005). These phenomena consist in  
11 sudden mass movements of a mixture of water and granular material that rapidly develop  
12 downslope eroding the soil cover and increasing their original volume (Iovine et al., 2003).  
13 Due to their high destructiveness, the study of these processes is an important research topic  
14 that can support decision makers in developing more detailed land-use maps and landslide  
15 hazard mitigation plans.

16 However, it is not simple to predict the probability of occurrence and magnitude of shallow  
17 landslides, considering the complexity of the phenomenon, mostly related to the variability of  
18 controlling factors (e.g. geology, topography, climate and hydraulic conditions, etc.). In this  
19 respect, a relation between triggering events (i.e. rainfall) and landslide occurrences is needed.  
20 To evaluate this cause-effect relationship, an approach widely used in the literature relies on  
21 the definition of empirical thresholds (Caine, 1980; Reichenbach et al., 1998; Wieczorek and  
22 Glade, 2005; Guzzetti et al., 2007). An empirical threshold defines the rainfall, soil moisture  
23 or hydrological conditions that, when reached or exceeded, are likely to trigger landslides  
24 (Reichenbach et al., 1998). Rainfall intensity-duration thresholds for the possible occurrence  
25 of landslides are defined through the statistical analysis of past rainfall events that have  
26 resulted in slope failures, and can be classified on the basis of the geographical extent for  
27 which they are determined (i.e. global, national, regional or local thresholds) and the type of  
28 rainfall information used to establish the threshold (Brunetti et al., 2010).

29 Nonetheless, the reliability of empirical thresholds is generally affected by quality and  
30 availability of the historical data. In fact, adequate historical data on landslides and  
31 simultaneous rainfall are in most cases available only for a relatively short period, which may  
32 not be sufficiently significant from a statistical point of view. Furthermore, rainfall intensity

1 and duration alone may not be able to capture most of the uncertainty related to landslide  
2 triggering (Peres and Cancelliere, 2014). Another drawback of the empirical rainfall  
3 thresholds is a general lack in spatial resolution. This aspect cannot be neglected if we  
4 consider that the terrain factors which control the onset of instability during a rainfall event  
5 can vary spatially to such an extent that, from a theoretical point of view, the rainfall  
6 threshold can be different for each landslide (Lo et al., 2012). Finally, further criticisms are  
7 based on the observation that it is not the amount of precipitation but the (largely unknown)  
8 amount of water that infiltrates and moves into the ground to cause failure (Guzzetti et al.,  
9 2008).

10 For this reason, in recent years different models have been developed to define physical  
11 (process-based) thresholds. Specifically, these models can determine the amount of  
12 precipitation needed to trigger slope failures, as well as the location and time of expected  
13 landslides, using spatially variable characteristics (e.g. slope gradient, soil depth and shear  
14 resistance) with a simplified dynamic hydrological model that predicts the pore pressure  
15 response to rainfall infiltration (Montgomery and Dietrich, 1994; Wilson and Wieczorek,  
16 1995; Terlien, 1998; Frattini et al., 2009). These models, although they are challenging to  
17 apply over large areas where a detailed knowledge of input parameters is very difficult to  
18 acquire (Berti et al., 2012), are usually calibrated using rainfall events for which rainfall  
19 measurements and the location and time of slope failures are known.

20 In this paper we propose an approach based on TRIGRS (Baum et al., 2002), a physically-  
21 based model that predicts the timing and distribution of shallow, rainfall-induced landslides  
22 combining an infinite slope stability calculation with a transient, one-dimensional analytic  
23 solution for pore-pressure response to rainfall infiltration. This model has been used in order  
24 to define different shallow landslide triggering scenarios in the study area (located SW of  
25 Messina in north-eastern Sicily, Italy) by varying the rainfall input on the basis of the results  
26 deriving from the analysis of the historical rainfall data. Prior to this stage, the model has been  
27 thoroughly validated through the back-analysis of the disaster occurred in the same area on 1  
28 October 2009. On that day, a heavy rainstorm triggered several hundreds of shallow  
29 landslides, causing 37 fatalities and severe damage to buildings and infrastructure (Schilirò  
30 and Esposito, 2013). Given the nature of the event, it can be considered particularly  
31 representative of the studied phenomenon and, thus, suitable for testing the reliability of the  
32 physically-based model.

1 The paper is organized as follows: after a brief description of the study area and the 1 October  
2 2009 event (Sect. 2), a summary of the landslide/flood events occurred in the past is reported  
3 (Sect. 3). Then, the methods used for the parameterization of TRIGRS model and the analysis  
4 of the historical rainfall data are outlined (Sect. 4). Afterwards, the results of the back-  
5 analysis of 2009 event and the evaluation of possible future triggering scenarios are provided  
6 (Sect. 5) and discussed, along with the main features of the proposed approach (Sect. 6).  
7 Finally, in Sect. 7 the main conclusions are summarized.

8

## 9 **2 General features of the study area and the 1 October 2009 event**

10 The study area (Fig. 1) is located south of Messina (North-eastern Sicily, Italy), at the NE  
11 termination of the Peloritani Mountain Belt, that represents the southern border of the  
12 Calabrian-Peloritan arc. This chain is composed by different metamorphic units (Kabilo-  
13 Calabride Complex) of pre-alpine age and later involved in Hercynian and Alpine orogenic  
14 processes, and tectonically overlapping the sedimentary Maghrebian units (Lentini et al.,  
15 2000). Since the Late Miocene, the opening of the Tyrrhenian Basin led to the formation of an  
16 extensional fault system that involved and re-oriented some of the former structures. These  
17 faults, generally oriented NE-SW, have influenced the development of this region during the  
18 Pleistocene-Holocene (Antonioli et al., 2003; Di Stefano et al., 2012), resulting in a landscape  
19 characterized by steep slopes eroded by torrent-like straight watercourses, with alluvial  
20 conoids and debris-flow fans along the valleys. A thin (0.5 - 2 m) layer of colluvial deposits  
21 or coarse-grained regolith overlays the majority of the slopes, where small outcrops of marine  
22 terraces, documenting the different uplift-rates during the Late Pleistocene, can be found.  
23 Three orders of terraces can be distinguished at approximately 185, 135 and 95 m a.s.l.  
24 (Catalano and De Guidi, 2003), whereas there is no evidence of fluvial terraces. Catchments  
25 generally have small dimensions and markedly elongated shapes, with short time of  
26 concentration and direct discharge into the sea. In particular the study area, which has an  
27 extension of about 8 km<sup>2</sup> and a maximum height of about 700 m a.s.l., comprises three main  
28 catchments (Giampileri, Divieto and Racinazzo torrents), highly affected by the heavy  
29 rainstorm which occurred on 1 October 2009. This event was characterized by an extremely  
30 high rainfall amount in a few hours. For instance the Santo Stefano di Briga monitoring  
31 station, which is one of the rain gauges closest to the study area (Fig. 2a), recorded very high  
32 rainfall peaks (e.g. 18.5 mm of cumulated rain between 17:00 and 17:10 UTC) for a total of

1 225 mm of rain falling in just seven hours (i.e. between 14:00 and 21:00 UTC). The analysis  
2 of satellite data (Fig. 2b) highlights the marked localization of the weather system, also  
3 confirmed by the low rainfall values recorded in two rain gauge stations approximately 20 km  
4 from the study area (Antillo and Messina Istituto Geofisico monitoring stations, see Fig. 2a).  
5 Furthermore, it is worth noting that in the days preceding the event, the area was affected by  
6 two intense rainfall events: one on 16 September and one on the night between 23 September  
7 and 24 September. The cumulative rain in this period was approximately 300 mm and thus the  
8 total rainfall from 15 September to 1 October amounted to about 500 mm, which is 80 mm  
9 higher than the average October-December precipitation (421 mm), calculated from 79 years  
10 of historical pluviometric data recorded in Santo Stefano di Briga monitoring station. These  
11 data are directly available on the Sicily Region website (<http://www.osservatorioacque.it>).

12 As a consequence of such an extreme event, numerous shallow landslides were triggered;  
13 according to the classification by Hungr et al., 2014, such landslides can be classified as  
14 debris-flows (Fig. 3a) and debris-slides (Fig. 3b) that frequently evolved to debris-avalanches  
15 (Fig. 3c) (Trigila et al., 2015). According to Schilirò et al., 2015 between 15:00 and 17:00  
16 UTC the critical conditions rapidly developed due to a large increase in precipitation.  
17 Afterwards, first landslide events occurred: for instance, a witness asserts that the main  
18 debris-flow in Giampileri village would have occurred between 17:00-17:15 UTC. Finally,  
19 after a further rainfall peak (approximately at 18:00 UTC), many other shallow landslides  
20 were triggered in Giampileri and the surrounding areas. In particular, a devastating debris-  
21 flow suddenly rushed down the Racinazzo valley, crushing buildings, infrastructure and  
22 killing 14 people in Scaletta Marina village. On the other hand, similar events were recorded  
23 slightly later in Molino village, approximately between 18:30-18:45 UTC, due to the storm  
24 motion towards the inner areas. Landslide occurrences were reported until 20:00 UTC, after  
25 which no remarkable event would have occurred in the area. However, the experiences  
26 reported by witnesses along with the damage to buildings, both indicate very fast-moving  
27 debris-flows.

28

### 29 **3 Previous flooding and related events**

30 The regional climatic setting of north-eastern Sicily is typical Mediterranean, whereby rainfall  
31 is concentrated during the wet season (October-April), which is when extreme rainfall events  
32 generally occur. However, the local orographic control coupled with marine effect can highly

1 influence the occurrence and magnitude of such events. Furthermore, the particular drainage  
2 network of the area, characterized by low order streams with high gradient and short length,  
3 increases the energy of runoff waters during rainfall events, favouring the erosion processes  
4 and the transport of the loosened material, even of large dimensions. For these reasons, this  
5 part of Sicily has been affected in the past by recurring flood/landslide events. According to  
6 the results of an archival research, based on the review of technical reports from local  
7 Authorities, newspapers, local churches archives etc., about 46 landslide/flood events would  
8 have occurred since the 17<sup>th</sup> century, the most of which were during the autumn-winter period  
9 (Fig. 4). In this respect, it is worth mentioning the “quadruple rainstorm” that affected the  
10 whole Messina area on 13 November 1855, during which more than 100 people lost their  
11 lives due to the triggering of countless landslides and a widespread flooding (Cuppari, 1856).  
12 Extreme rainfall events affected this region also in recent years: in particular, an event similar  
13 to the 1 October 2009 one occurred just two years before, on 25 October 2007. On this day,  
14 approximately 134 mm of rain fell in the area, and this event also featured extremely high  
15 intensity peaks (i.e. 29.1 mm in 10 minutes). The damage to buildings and infrastructure was  
16 remarkable; however, unlike the 1 October event, there were no casualties (Aronica et  
17 al.,2008). Heavy rainstorms hit the area also after the 1 October 2009 event, i.e. in the night  
18 between 9 and 10 March 2010 and on 1 March 2011. During these events several landslides  
19 were triggered in Scaletta Marina and Giampilieri, convincing the authorities to declare the  
20 state of natural disaster for the villages of southern Messina area. However, even though the  
21 increase of recorded events during the last twenty years also depends on the increasing  
22 number of sources of information, it is important to emphasize that, in the same period, the  
23 landslide risk exposure of the area has increased, substantially due to the enlargement of the  
24 urban area as a consequence of poor land-use planning (Del Ventisette et al., 2012). Finally,  
25 recent studies (Bonaccorso et al., 2005; Arnone et al., 2013) indicate an increasing trend for  
26 extreme, short-duration rainfall events over the last few decades in Sicily, especially in  
27 coastal areas.

28

#### 29 **4 Methodology**

30 As mentioned above, the approach proposed in this paper consists of two stages:

- 31 1) Back-analysis of the 1 October 2009 event;
- 32 2) Evaluation of different triggering scenarios

1 As regards the first step (Fig. 5), we compared the Safety Factor (FS) map obtained by using  
2 TRIGRS, a well-known regional, physically-based stability model (Sect. 4.1), with the  
3 inventory map of the landslides triggered during the event. In this respect, it is important to  
4 note that for each of more than 700 mapped landslides, identified through analysis of high  
5 resolution aerial orthophotos integrated by field surveys in the days after the event, the  
6 landslide deposit has been distinguished from the source area (Trigila et al., 2015). Therefore,  
7 in order to achieve more accurate assessment, only the source areas have been used for the  
8 comparison with the numerical simulations. The input parameters of the numerical model (i.e.  
9 soil thickness, spatial rainfall rate, hydraulic conditions and geotechnical properties of the  
10 colluvial deposit) have been evaluated by means of lab tests, empirical methods and  
11 numerical simulations (Sect. 4.2). In the next step, for the reconstruction of different  
12 triggering scenarios we used specific rainfall inputs, whose return period (RP) has been  
13 defined through a statistical analysis of the historical rainfall data available for the study area  
14 (Sect. 4.3).

15

#### 16 **4.1 Theoretical basis of TRIGRS model**

17 TRIGRS (Transient Rainfall Infiltration and Grid-based Slope Stability model) is a Fortran  
18 program designed for modelling the timing and distribution of shallow, rainfall-induced  
19 landslides. It combines a transient, one-dimensional analytic solution for pore-pressure  
20 response to rainfall infiltration with an infinite slope stability calculation. In the original  
21 version (Baum et al., 2002), the infiltration model was based on Iverson's (2000) linearized  
22 solution of Richards' equation, with implementation of complex storm histories, an  
23 impermeable basal boundary at finite depth and a simple runoff routing scheme (Savage et al.,  
24 2003; Salciarini et al., 2006). Introducing a time-varying rainfall input on the ground surface  
25  $I_z(t)$ , the pressure head response  $\Psi(Z,t)$  can be computed using the following input parameters  
26 (locally variable throughout the model): slope, soil layer depth  $d_{lb}$ , depth of the initial steady-  
27 state water table  $d_{wt}$ , long term (steady-state) surface flux  $I_{ZLT}$  and saturated hydraulic  
28 conductivity  $K_s$ . However, this solution is appropriate for initial conditions where the  
29 hillslope is tension-saturated (Fig. 6a). In the second version (Baum et al., 2008), TRIGRS  
30 model was expanded to address infiltration into a partially unsaturated surface layer above the  
31 water table by using an analytical solution of the Richards' equation for vertical infiltration  
32 (Fig. 6b). TRIGRS uses four hydrodynamic parameters to linearize the Richards' equation

1 through the unsaturated zone, according to the hydraulic model proposed by Gardner (1958):  
 2 the saturated ( $\theta_s$ ) and residual ( $\theta_r$ ) water content, the saturated hydraulic conductivity ( $K_s$ ) and  
 3 a specific parameter linked to the pore size distribution ( $\alpha_G$ ). If the amount of infiltrating  
 4 water reaching the water table exceeds the maximum amount that can be drained by gravity,  
 5 TRIGRS simulates the water-table rise comparing the exceeding water quantity to the  
 6 available pore space directly above the water table or capillary fringe and then, for each time  
 7 step, applies the water weight at the initial top of the saturated zone to compute the new  
 8 pressure head (Baum et al., 2010). For the calculation of the Safety Factor in the unsaturated  
 9 configuration, the pressure head is multiplied by the effective stress parameter, as suggested  
 10 by Vanapalli and Fredlund, 2000:

$$11 \quad \chi = (\theta - \theta_r) / (\theta_s - \theta_r) \quad (1)$$

12 where  $\theta$  is the soil water content. This approximation has application to a generalized  
 13 effective stress law and represents a simplified form of the suction-stress characteristic curve  
 14 (Lu and Godt, 2008; Lu et al., 2010). Considering the presence of a thin layer of colluvial  
 15 deposits over the metamorphic bedrock, in this work we assume a finite depth for the  
 16 impermeable basal boundary and initially unsaturated conditions for the regolith.

17

## 18 **4.2 Parameterization of the numerical model**

19 In order to define the input parameters of TRIGRS model, use was made of different methods  
 20 and techniques. To estimate the spatial variation of soil thickness, the model proposed by  
 21 Saulnier et al., 1997 has been applied to the study area (Fig. 7a). This model correlates soil  
 22 depth to the local slope angle according to the following equation:

$$23 \quad h_i = h_{\max} \left\{ 1 - \left[ \frac{\tan \alpha_i - \tan \alpha_{\min}}{\tan \alpha_{\max} - \tan \alpha_{\min}} \left( 1 - \frac{h_{\min}}{h_{\max}} \right) \right] \right\} \quad (2)$$

24 where  $h_i$  is the soil thickness computed at pixel  $i$ ,  $h_{\max}$  and  $h_{\min}$  are the maximum and  
 25 minimum soil thickness values measured in the area,  $\alpha_i$  is the slope value at pixel  $i$ , while  $\alpha_{\max}$   
 26 and  $\alpha_{\min}$  are the maximum and minimum slope values encountered in the study area. The  
 27 maximum and minimum values of slope and soil thickness, which were measured within the  
 28 source areas of the shallow landslides triggered during the 1 October 2009 event, are equal to  
 29  $58^\circ$ - $17^\circ$  and 1.5-0.5 m respectively, and they can be considered reliable since the 2009



1 landslides mostly involved the entire soil profile. Although the model proposed by Saulnier et  
2 al., 1997 relies heavily on geomorphological simplifications, it is frequently used to estimate a  
3 spatially distributed soil depth field in basin scale modelling (e.g. Salciarini et al., 2006).

4 To reproduce the spatial rainfall distribution of the 1 October 2009 rainstorm, the conditional  
5 merging technique (Ehret, 2002; Pegram, 2003) has been chosen as interpolating method. In  
6 this approach, the information from the satellite radar is used to condition the spatial rainfall  
7 field obtained by the interpolation of rain gauge measurements. Although there are numerous  
8 deterministic methods for estimating spatial rainfall distribution (e.g. Thiessen polygon,  
9 Inverse Distance Weighted, polynomial interpolation, etc.), geostatistical methods are  
10 commonly preferred because they allow not only to account for spatial correlation between  
11 neighboring observations to estimate values at ungauged locations, but also to include more  
12 densely sampled secondary attributes (i.e. weather radar data) with sparsely sampled  
13 measurements of the primary attribute (i.e. rainfall) to improve rainfall estimation (Mair and  
14 Fares, 2011). In particular, meteorological satellite radars give a large-scale vision of  
15 precipitation fields compared to scattered point estimates from rainfall gauges. In this study,  
16 use was made of the precipitation rate maps deriving from the processing of EUMETSAT  
17 (European Organisation for the Exploitation of Meteorological Satellites) satellite data. These  
18 maps, that were made available by the National Center of Aeronautical Meteorology and  
19 Climatology (CNMCA) of the Italian Air Force, are generated from blending of PMW  
20 (passive microwave) measurements and IR (Infrared) brightness temperatures, coupled with  
21 the NEFODINA (DYNAMIC NEFOanalysis) software, that allows the automatic detection  
22 and classification of convective cloud systems reducing the underestimation of precipitation  
23 (Mugnai et al., 2013). Ten-minute rainfall records of six stations (Antillo, Colle San Rizzo,  
24 Fiumedinisi, Ganzirri, Messina Istituto Geofisico and Santo Stefano di Briga) have been used  
25 as input data, after conveniently converting them into fifteen-minute data for the comparison  
26 with the corresponding radar rainfall maps. Thus, sequential rainfall maps (Fig. 7b) have been  
27 obtained referred to the time period between 13:00 and 21:00 UTC.

28 The hydraulic properties of the colluvial deposit, the steady-state water-table depth and the  
29 initial soil moisture conditions have been estimated using HYDRUS 1-D model (Šimůnek et  
30 al., 1998), a USDA (United States Department of Agriculture) Salinity Laboratory software  
31 which can simulate the water flow into unsaturated porous media resulting from a rainfall  
32 event. The software describes infiltration in vadose zone using a modified version of

1 Richards' equation. In this paper, numerical simulations have been performed for the period  
2 1-30 September 2009 in order to quantify the effect of the 1-month antecedent rainfall on soil  
3 moisture conditions. As hydraulic model, van Genuchten-Mualem model (van Genuchten,  
4 1980) was chosen to simulate the water flow, whereas the hydrodynamic parameters  $\theta_s$ ,  $\theta_r$ ,  $\alpha_G$   
5 and  $K_s$  are predicted from soil grain size distribution using the ROSETTA Lite module  
6 (Schaap et al., 2001). This module uses a database of measured water retention and other  
7 properties for a wide variety of media. For a given grain size distribution and other soil  
8 properties the model estimates a retention curve (i.e. the relationship between soil water  
9 suction  $\Psi$  and the amount of water remaining in the soil  $\theta$ ) with good statistical comparability  
10 to known retention curves of other media with similar physical properties (Nimmo, 2005).  
11 Daily rainfall data have been used as input for the model, whereas evapotranspiration is  
12 accounted for by inserting into the Hargreaves equation (Jensen et al., 1997) the maximum  
13 and minimum temperature values recorded during the investigated period. As lower  
14 boundary, a zero-flux condition was assumed due to the presence of an impermeable bedrock  
15 below the soil cover. A 80-cm soil profile inclined of  $38^\circ$  (i.e. the average soil thickness and  
16 slope observed within the landslide source areas) was chosen as the most representative  
17 geometric configuration of the slope prior to 1 October event.

18 Laboratory tests have been performed to measure physical and mechanical properties of the  
19 colluvial deposit (Table 1). The grain size distribution analyses show a soil composed mainly  
20 of coarse-grained particles (gravel and sand) with minor components of silt and clay. With  
21 regard to the mechanical parameters, drained triaxial tests have been conducted on three large  
22 reconstituted specimens ( $H=200$  mm,  $D=100$  mm). To reconstitute each specimen, the soil  
23 was compacted inside a mould in different layers of decreasing depth, in order to account for  
24 under-compaction. The tested material was sieved leaving the maximum grain size of 10 mm  
25 and imposing 35% of porosity (i.e. the average porosity obtained from different soil samples)  
26 and 8% of initial water content. The latter value can be considered representative of the  
27 investigated soil on the basis of the results of HYDRUS 1-D model (see Sect. 5.1). For the  
28 same material other authors (Aronica et al., 2012; Peres and Cancelliere, 2014; Penna et al.,  
29 2014) reported values which vary between  $30^\circ$  and  $40^\circ$  for the friction angle and between 0  
30 and  $5 \text{ kN m}^{-2}$  for the cohesion; thus the resulting internal friction angle (i.e.  $36.3^\circ$ ), obtained  
31 by assuming a null cohesion, substantially agrees with these values. However, it is important  
32 to stress that this difference can depend on both the natural spatial variability of soil shear

1 strength parameters and the type of deposit, characterized by an extremely variable texture  
2 resulting from erosion and weathering areas.

3

#### 4 **4.3 Analysis of historical rainfall data**

5 In order to depict different shallow landslide triggering scenarios in the study area, firstly it is  
6 necessary to evaluate the recurrence of specific rainfall events, which can be used as input for  
7 the physically-based model. Therefore, a statistical analysis of historical rainfall data has been  
8 performed. The hydrological-statistical model is based on the analysis of the maximum values  
9 assumed by the chosen hydrological variable (i.e. cumulative rainfall at different time  
10 intervals). Depending on the type of considered rainfall event (i.e. prolonged or intense short-  
11 duration rainfall), the hydrological variables are identified and then the recurrence of the  
12 event can be expressed in terms of return period (RP). In this study the probability model  
13 relied on the Generalized Extreme Value (GEV) distribution introduced by Jenkinson (1955).  
14 This distribution is a generalized version of the more known Gumbel distribution, which is  
15 largely used in the study of extreme events. The variables of “cumulative rainfall” ( $PC_n$ ) i.e.,  
16 in 1, 2, 5, 10, 30, 60, 90, 120 and 180 days are computed from daily rainfall data by means of  
17 the expression:

$$18 \quad PC_{n,j} = \sum_{i=j-n+1}^j P_i \quad \text{with } n = 1, 2, 5, 10, 30, 60, 90, 120, 180; \quad (3)$$

19 where  $j$  is the progressive number of days that form the analyzed time interval and  $P_i$  is the  
20 rainfall value recorded the  $i$ -th day. The maximum values of each variable are extracted, year  
21 by year, from the datasets so generated and the parameters of the GEV function are  
22 determined from the above values, by applying the Probability Weighted Moments (PWM)  
23 method introduced by Greenwood et al. (1979) and subsequently modified by Hosking et al.  
24 (1985). Finally, the inversion of the probability function yields the values of cumulated  
25 rainfall  $x$  for each of the variables (1, 2, 5, 10..... 180 days) and for different RPs. Then, these  
26 values are interpolated with a view to build the rainfall probability curves.

27 To yield reliable results, this type of analysis requires sufficiently long and continuous time  
28 series of rainfall data (at least 20 years of recorded data according to Houghton et al. 2001 and  
29 Serrano, 2010). For this reason, use was made of daily rainfall data from Santo Stefano di  
30 Briga and Messina Istituto Geofisico rainfall stations, that are operational since 1925 and

1 1952, respectively. However, if we consider that the extreme rainfall events which  
2 periodically affect the study area are usually of short duration, as in the case of the 1 October  
3 2009 event, it would be extremely interesting to analyze the historical data of maximum  
4 hourly rainfall intensity. Unfortunately, these data are not available for the above mentioned  
5 stations. For this reason, use was made of hourly rainfall data (i.e. cumulated in 1, 3, 6, 12 and  
6 24 hours) from Ali Terme station, that is located approximately 4 km SE of Fiumedinisi  
7 station (see Fig. 12b); thus, this station has been considered sufficiently close to be used to  
8 assess the recurrence of the rainfall events recorded in Fiumedinisi station.

9

## 10 **5 Results**

### 11 **5.1 Back-analysis of the 1 October 2009 event**

12 As previously mentioned, before applying the TRIGRS model to back-analyze the 1 October  
13 2009 event, it was necessary to evaluate the soil moisture conditions prior to the event  
14 through HYDRUS 1-D model. According to the simulation results obtained by using the grain  
15 size distribution of the sample n.1 (see Table 1), the absence of a steady-state water table  
16 within the soil cover can be assumed, whereas in Fig. 8a the resulting volumetric water  
17 content trend with depth at four different times (1, 24, 25 and 30 September) is reported. The  
18 initial soil moisture ( $\theta = 0.047$ ) is assumed near to the residual water content value considering  
19 the hot, dry conditions during the preceding summer months. The effect of the September  
20 rainfall (Fig. 8b) results in a progressive increase in soil water content, that is equal to 0.194  
21 on 25 September (the day after the second rainfall event, see Table 2). It is worth noting that  
22 in the lower part of the soil profile the water content progressively increases over the days,  
23 due to the advance of the wetting process, resulting in an average value of 0.19 on 30  
24 September, which corresponds to a gravimetric water content ( $w$ ) of approximately 10.8%  
25 and a degree of saturation ( $S_r$ ) equal to 54.4% (on the basis of the physical properties reported  
26 in Table 1).

27 Once the initial soil moisture conditions are estimated, all the input parameters required by  
28 TRIGRS can be defined (Table 3). As digital elevation model, use was made of a detailed (2 x  
29 2m) pre-event DEM, resampled at the 4 x 4m resolution substantially due to limitations on  
30 computing time. Soil thickness ( $H$ ) and rainfall rate ( $I_z$ ) vary from cell to cell on the basis of  
31 maps obtained through the methods described in Sect. 4.2. According to the available data an

1 average friction angle of  $35^\circ$  has been used, whereas the cohesion has been progressively  
 2 increased to  $3 \text{ kN m}^{-2}$  so that only very few cells (i.e. 260, which represent about 0.04% of all  
 3 grid cells in the study area) result unstable before the beginning of the event. In any case, the  
 4 chosen value lies within the range of values reported by other authors for the same material  
 5 (see Sect. 4.2). The depth-averaged soil unit weight ( $\gamma_n$ ) is equal to  $19.22 \text{ kN m}^{-3}$  given the  
 6 porosity (35%), the degree of saturation (54.4%) and the unit weight of soil solids ( $26.73 \text{ kN}$   
 7  $\text{m}^{-3}$ ), while  $\theta_s$  (saturated water content),  $\theta_r$  (residual water content) and  $K_s$  (saturated hydraulic  
 8 conductivity) are directly predicted using HYDRUS-1D model. Given the absence of an  
 9 initial water table, its depth ( $d_{wt}$ ) so corresponds to the bedrock-soil interface. To evaluate  $\alpha_G$   
 10 parameter, that is typical of Gardner hydraulic model, use was made of the conversion  
 11 formula introduced by Ghezzehei et al., 2007 which defines a correspondence between  
 12 Gardner and van Genuchten-Mualem models through the capillary length approach (Warrick,  
 13 1995). On the basis of the results of the same simulations the  $I_{ZLT}$  parameter, that represents  
 14 the long-term background rainfall rate, was assumed equal to the cumulative actual surface  
 15 flux value ( $8.49 \times 10^{-8} \text{ m s}^{-1}$ ). Finally, the saturated hydraulic diffusivity ( $D_0$ ) has been  
 16 calculated according to:

$$17 \quad D_0 = \frac{(K_s H)}{S_y} \quad (4)$$

18 where  $K_s$  is the saturated hydraulic conductivity,  $H$  the average soil thickness (80 cm) and  $S_y$   
 19 the specific yield (Grelle et al., 2014). If we consider that the investigated soil can be  
 20 classified as loamy sand, the specific yield has been assumed equal to 0.34, on the basis of  
 21 typical values given by Johnson, 1967 (also reported in Loheide II et al., 2005) for each soil  
 22 textural class.

23 With regard to the comparison between the numerical simulations and the landslide inventory  
 24 map, Table 4 reports, as well as the number and relative percentage ( $P_U$ ) of predicted unstable  
 25 pixels (i.e.  $FS \leq 1$ ), the percentage of correctly predicted landslide ( $P_L$ ) and stable ( $P_S$ ) pixels  
 26 between 13:00 and 21:00 UTC. Fig. 9 shows the temporal evolution of slope instability at the  
 27 catchment scale: only 0.2% of pixels are indicated as unstable at 13:00 UTC (beginning of the  
 28 rainfall event). After a progressive increase in the following four hours, the instability rapidly  
 29 rose between 17:00 and 18:00 UTC ( $P_U$ : +21.2%) in correspondence of a rainfall peak, and  
 30 the critical stage continued until 21:00 UTC, given that  $P_U$  passed from 39.6% to 100% in just  
 31 3 hours. This temporal evolution of the phenomenon substantially agrees with the witnesses,

1 although during the real event no particular increase of slope instability has been recorded  
2 after 20:00 UTC. To fully evaluate the accuracy of the model, a ROC (Receiver Operating  
3 Characteristics) curve analysis has been performed by comparing the final FS map (21:00  
4 UTC) with the landslide inventory. The ROC curve measures the goodness of the model  
5 prediction plotting, for different threshold values, the True Positive rate, i.e. the proportion of  
6 correctly predicted positive values ('landslide presence') and the False Positive rate, i.e. the  
7 proportion of negative values ('landslide absence') erroneously reported as positive. The Area  
8 Under Curve (AUC), which varies from 0.5 (diagonal line) to 1, quantifies the predictive  
9 capability of the model.

10 According to the results, the FS map correctly classifies 68.8% of source areas (True Positive)  
11 and 75.1% of stable areas (True Negative) with  $FS = 1$ , whereas the AUC is equal to 0.795  
12 (Fig. 10a). However, due to the great variability of the soil texture, three different grain size  
13 distributions are available (Table 1), but the back-analysis has been performed using the grain  
14 size characteristics of the sample n.1 only. This choice can be explained analyzing the  
15 simulation results obtained accounting for the grain size distributions of the other two  
16 samples. With regard to the parameters derived from HYDRUS 1-D (Table 5), it can be noted  
17 that the saturated hydraulic conductivity and consequently the hydraulic diffusivity can differ  
18 by up to an order of magnitude, due to the presence of larger quantity of fine material (silt and  
19 clay) in sample n.2 and n.3. On the contrary, the other parameters are substantially similar for  
20 all the three samples. By using these parameters in TRIGRS simulations, a different  
21 reconstruction of the 2009 event is obtained (Fig. 10b). Although the maximum number of  
22 unstable pixels is similar in the case of sample n.1 and sample n.2, in the second one the  
23 instability peak occurs far too late compared to the real event (approximately at 5.00-6.00  
24 UTC of the following day). On the contrary, for sample n.3 the low value of hydraulic  
25 conductivity causes not only a delay of the instability even greater, but also a lower number of  
26 unstable pixels at maximum instability, which develops in a larger time interval  
27 (approximately between 9.00 and 13.00 UTC of 2 October). For these reasons, we consider  
28 the parameters obtained according to the grain size characteristics of sample n.1 as the most  
29 representative of the investigated soil.

30

## 5.2 Rainfall probability curves and return period of the 1 October 2009 event

Figure 11a-b shows the graphic comparison between cumulative frequency (symbols) and GEV probability function (continuous line), obtained by using the daily rainfall records from Santo Stefano di Briga and Messina Istituto Geofisico stations. As it can be observed, the good fitting between data and probability function confirms the reliability of the applied method. With regard to the probability curves (Fig. 11c-d), the comparison reveals that the highest rainfall values are attributed to the Santo Stefano di Briga curves for the same RP. This finding emphasizes that, in the past, this station (the most representative of the sector most severely hit by the 2009 event) has recorded more intense and severe rainfall events than the other one. On the basis of the same curves, the RPs of the rainfall accumulated up to 1 October 2009 have been estimated (Table 6). An estimation has been made also for the rainfall accumulated up to 30 September (i.e. the day prior to the event), but the obtained values infer that the rainfall amount, at both stations, is far from exceptional (estimated RPs = 1 year); thus, rainfall prior to the event practically lies within the standard range, in contrast with rainfall accumulated up to 1 October. In this case, while rainfall recorded at Messina Istituto Geofisico continues to be unexceptional (estimated RP = 4-5 years), rainfall accumulated in a single day (1 October) at Santo Stefano di Briga has a RP = 47 years. This means that the event under review was not only strongly localized in space, but also particularly severe in that specific sector. This finding is also substantiated by what has been previously pointed out, i.e. the highest RPs have been obtained for the station with the highest rainfall probability curves.

With regard to the analysis of the historical data of maximum hourly rainfall intensity from Ali Terme station, the results shows that the fit between cumulative frequency and probability (Fig. 12a) is not as good as in the preceding analyses. However, it is worth stressing that data about intense precipitation are generally scantier than daily ones and that the resulting statistical analyses are usually less reliable. The resulting rainfall probability curves (Fig. 12b) define a RP = 78 years for the 1-hour rainfall recorded on 1 October 2009 in Fiumedinisi station, a value greater than that estimated for the 1-day rainfall recorded in Santo Stefano di Briga station (47 years). Therefore, the 1-hour rainfall event can be classified as an extreme event. Nevertheless, it is particularly interesting to analyze the sub-event of maximum duration equal to three hours, a time after which major damage was observed in the area. In this case the estimated RP is equal to 26 years (Table 7): this value infers that, even if the RP

1 of the 1-hour rainstorm allows to assert that it was an extreme event, the 3-hour sub-event is  
2 characterized by a RP much lower, which suggests its classification as not severe. However, it  
3 is worth noting that the probabilistic analysis is affected by several uncertainties, related to  
4 the type of probabilistic model and the definition of the parameters of the model itself.  
5 Generally speaking, the uncertainty tends to increase with decreasing the sample size (i.e. the  
6 number of measurement years) and increasing the considered RP.

### 7 **5.3 Evaluation of different triggering scenarios**

8 Once the physically-based model was validated through the back-analysis of the 1 October  
9 2009 event, different TRIGRS simulations have been performed by varying the rainfall input,  
10 on the basis of the rainfall probability curves described above. With regard to the other input  
11 parameters of the model, those used for the analysis of the 1 October event have been kept. It  
12 is important to note that only hourly simulations have been performed. In fact, if we  
13 reproduce the 2009 event and compare the simulation results obtained by using the 1-day  
14 rainfall value with those gained with the 15-minute rainfall maps, it results a much lower  
15 number of predicted unstable pixels in the first case (5,405) rather than in the second  
16 (126,207). Therefore, daily data are not suitable for this type of analysis, due to the excessive  
17 underestimation of the instability phenomena. In the hourly simulations four rainfall values,  
18 which correspond to four different RPs (i.e. 2, 4, 10 and 20 years) have been used, in such a  
19 way as to evaluate the effect of more frequent rainfall events with respect to the 2009 one.  
20 Table 8 shows the number of unstable pixels at the end of the simulated rainfall event and in  
21 the next two hours. In this way, it can be noted that the increase of instability continues up to  
22 one hour after the end of the rainfall, specifically for infiltration rates not less than  $15 \text{ mm h}^{-1}$ .  
23 This aspect can be explained considering that water needs a certain time to reach greater  
24 depths, so that even the deeper and flatter grid cells may become unstable. The results also  
25 emphasize the importance, in terms of produced instability, of the 1-hour and 3-hour rainfall  
26 amount even for relatively low RPs (i.e. 10-20 years). For instance, a 3-hour rainfall with RP  
27 = 10 years would cause about half (48.9%) of the slope instability calculated for the entire 1  
28 October event. In the case of 6-hour rainfalls, a significant level of instability develops only  
29 for events with  $\text{RP} \geq 20$  years, while with events of longer duration (12 hours) the number of  
30 predicted unstable pixels is extremely low even for relatively high RPs. Therefore, the  
31 duration of a rainfall event can produce completely different triggering scenarios for equal  
32 rainfall amount. In this respect, we used two different rainfall inputs (i.e. 45 and 85 mm)



1 whose RP varies depending on the duration of the event (i.e. 1 or 3 hours), in order to analyze  
2 the variation of FS and pressure head over time at the same grid cell of interest (Figure 13).  
3 The elevation and slope value of the cell (i.e. 320 m a.s.l. and 38°) correspond to the average  
4 values observed within the landslide source areas. The results shows that the FS decrease (and  
5 consequently the increase of the pressure head measured at the same depth) is greater and  
6 more rapid in the case of 1-hour rainfall events, due to the greater rainfall rate. Furthermore,  
7 also in this analysis the increase of instability occurs in the hour following the event. In this  
8 sense, the maximum variations are observed in the 85 mm/1-hour rainfall, in which FS and  
9 pressure head pass from 0.96 to 0.9 and from 0.08 to 0.14 m, respectively. On the contrary, in  
10 all the four cases a very slow recovery of the preceding stability conditions can be noted over  
11 the two hours after the instability peak.

12

## 13 **6 Discussion**

14 The results obtained from the numerical simulations confirm not only the need of hourly  
15 analyses for extreme but short duration rainfall events, but also the influence of 1-hour and 3-  
16 hour rainstorms on the slope stability conditions, at least in the study area. In this respect, if  
17 we observe the characteristics of the 1 October 2009 event, we can distinguish a main phase  
18 of approximately six hours (15:00-21:00 UTC) with a 1-hour rainfall peak (17:00-18:00  
19 UTC), thus numerical simulations not exceeding 6 hours can be considered sufficiently  
20 representative of the real phenomenon. However, the results reported in Table 9 indicate that  
21 the 3-hour sub-event would have produced approximately the same instability of the 6-hour  
22 rainfall amount (73.2% vs. 74.3%). This means that the 3-h sub-event alone would have  
23 caused almost all landslides, and if we consider that this event is characterized by a relatively  
24 low return period (26 years), it can be understood how such instability phenomena are likely  
25 to occur in this area. The same statements can be inferred by simulating a preceding landslide  
26 event occurred on 25 October 2007 (Table 9). On the basis of the evidence, this event is  
27 comparable to the 2009 one (see Sect. 3) and the 3-hour sub-event, characterized by a similar  
28 RP (30 years) produces, in fact, a similar level of instability (84.4% of the slope instability  
29 calculated for the 2009 event). However, analyzing the event on a 6-hour scale, once again a  
30 slightly underestimation of the entire event is observed, according to the decrease of the  
31 percentage of unstable pixels (73.6%). Although the 1-hour rainfall amount is lower in the  
32 2007 case (65 mm vs. 85 mm), the fact that both 1-hour and 3-hour rainstorms with relatively

1 low RP can cause a substantial instability level emphasizes the severity of recurring rainfall  
2 events in the study area and explain the high number of landslide/flood events occurred in the  
3 past (see Sect. 3). In fact, considering the high values that characterize the rainfall probability  
4 curves of Ali Terme rain gauge station (see Sect. 5.2), we can assert that short duration  
5 rainfall events frequently have a high intensity in this specific area. Therefore the combination  
6 of recurring and heavy rainfall events, probably due to specific geomorphological and  
7 climatic features that influence the development of localized severe storms, justifies the  
8 approximately 40 landslide/flood events that would have occurred since the last century in  
9 this area.

10 From a methodological point of view, it is worth noting how the approach proposed in this  
11 paper (Fig. 14) combines various techniques and methods optimizing different types of data,  
12 depending on their availability. For instance, the parameterization of the physically-based  
13 model can be performed both in the absence and presence of preceding reference events. In  
14 the former case, only the geotechnical parameters and the soil thickness are needed, while in  
15 the latter the process used for the back-analysis of the 1 October 2009 event can be applied to  
16 any other event. Here, in particular, it is important to stress that the comparison with a  
17 preceding landslide event allows to increase the reliability of the model, as long as a  
18 comprehensive and detailed event-based landslide inventory exists. With regard to the  
19 evaluation of the initial soil conditions, in this study the HYDRUS 1-D model has been used  
20 considering the 1-month antecedent rainfall. However, some recent studies have investigated  
21 the linkage between soil moisture and landslide occurrence by using soil moisture data  
22 derived by in situ (Baum and Godt, 2009; Hawke and McConchie, 2011) and satellite sensors  
23 (Ray and Jacobs, 2007; Ray et al., 2010), and this type of measurements, if available, can be  
24 used to define the input parameters of the model. The last step of the approach concerns the  
25 definition of the rainfall input to be used for the evaluation of a specific triggering scenario.  
26 By means of a statistical analysis of hourly rainfall data, different rainfall values having  
27 different RPs may be used to depict different scenarios, to changing the initial soil conditions  
28 and the duration of the rainfall input. However, as emphasized in the discussion of the results,  
29 establishing which is the critical rainfall duration that triggers the shallow landslides cannot  
30 be straightforward, because completely different slope stability conditions can be obtained  
31 with different combinations of single rainfall inputs within the same rainfall event, even with  
32 the same initial soil conditions. For this reason, and considering the chance to use also soil  
33 moisture data, a possible application of the here-proposed approach could be to develop an

1 early warning system based on rainfall thresholds, identified by the physically-based model  
2 validated according to the above-described process. In this way, a model in which the initial  
3 conditions are constantly updated, could depict more consistent and reliable triggering  
4 scenarios, by using any rainfall event forecasted for the next hours.

5

## 6 **7 Conclusions**

7 In this study, we introduce an approach for the analysis of shallow landslide triggering  
8 scenarios that uses the TRIGRS code, a physically-based model which describes the stability  
9 conditions of natural slopes in response to specific rainfall events. As a first step, the model  
10 has been validated through the back-analysis of a reference landslide event, i.e. the disaster  
11 occurred in the southern Messina area on 1 October 2009. Comparing the results of the  
12 numerical simulation with the 2009 landslide inventory, it turn out the model is able to  
13 reproduce quite well the reference event, both in terms of temporal evolution and spatial  
14 distribution of slope instability, identifying the areas mostly affected by shallow landslides. It  
15 is worth stressing that the model has been accurately parameterized through different methods  
16 and techniques, with specific focus on the evaluation of the spatial pattern of the triggering  
17 storm and initial soil moisture conditions.

18 Once the physically-based model has been validated, different triggering scenarios have been  
19 reconstructed by varying the rainfall input, on the basis of the rainfall probability curves  
20 obtained through a statistical analysis of historical rainfall data. The results indicate that the 1-  
21 day simulations strongly underestimate the landslide events triggered by extreme but short  
22 duration rainfalls (such as the 1 October one). With regard to the hourly analyses, it results  
23 that even recurring (RP = 10-20 years) 1-hour and 3-hour rainfall events can lead to  
24 significant slope instabilities. This feature confirms the destabilizing effect of recurring  
25 rainfall events in the study area, justifying the high number of landslide/flood events occurred  
26 in the past. As regards the proposed approach, the using of different techniques allows its  
27 application to different case studies, on the basis of the data availability. Furthermore, if we  
28 consider the possibility to depict constantly updated triggering scenarios, this approach could  
29 be used to develop specific landslide early warning systems, in order to support decision-  
30 makers in both risk prevention and emergency response.

31

1 **Acknowledgements**

2 The authors wish to thank an anonymous Referee for his/her helpful suggestions and  
3 constructive comments, which have largely contributed to improve the quality of the  
4 manuscript. The authors also wish to thank the Geostudi Srl. Laboratory (Rome, Italy) for  
5 performing the laboratory analyses of physical and mechanical properties of the colluvial  
6 deposit (report number 1718).

7

## 1 **References**

- 2 Antonioli, F., Kershaw, S., Rust, D., and Verrubbi, V.: Holocene sea-level change in Sicily  
3 and its implications for tectonic models: new data from the Taormina area, northeast Sicily,  
4 *Mar. Geol.*, 196, 53-71, doi: 10.1016/S0025-3227(03)00029-X, 2003
- 5 Arnone, E., Pumo, D., Viola, F., Noto, L.V., and La Loggia, G.: Rainfall statistics changes in  
6 Sicily, *Hydrol. Earth Syst. Sc.*, 17, 2449-2458, doi: 10.5194/hess-17-2449-2013, 2013
- 7 Aronica, G.T., Brigandì, G., Marletta, C., and Manfrè, B.: Hydrological and hydraulic  
8 analysis of the flash flood event on 25 October 2007 in North-Eastern part of Sicily, Italy,  
9 *Proceedings of Floodrisk 2008*, Oxford (UK), 2008
- 10 Aronica, G.T., Biondi, G., Brigandì, G., Cascone, E., Lanza, S., and Randazzo G.:  
11 Assessment and mapping of debris-flow risk in a small catchment in eastern Sicily through  
12 integrated numerical simulations and GIS, *Phys. Chem. Earth*, 49, 52-63, doi:  
13 10.1016/j.pce.2012.04.002, 2012
- 14 Baum, R.L., and Godt, J.W.: Early warning of rainfall-induced shallow landslides and debris  
15 flows in the USA, *Landslides*, 7, 259-272, doi: 10.1007/s10346-009-0177-0, 2009
- 16 Baum, R.L., Savage, W.Z., and Godt, J.W.: TRIGRS - A Fortran program for transient  
17 rainfall infiltration and grid-based regional slope-stability analysis, U.S. Geological Survey,  
18 *Open-File Report 02-424*, 61 pp., 2002
- 19 Baum, R.L., Savage, W.Z., and Godt, J.W.: TRIGRS - A Fortran program for transient  
20 rainfall infiltration and grid-based regional slope-stability analysis, version 2.0, U.S.  
21 Geological Survey, *Open-File Report 2008-1159*, 75 pp., 2008
- 22 Baum, R.L., Godt, J.W., and Savage, W.Z.: Estimating the timing and location of shallow  
23 rainfall-induced landslides using a model for transient, unsaturated infiltration, *J. Geophys.*  
24 *Res.*, 115, F03013, doi: 10.1029/2009JF001321, 2010
- 25 Berti, M., Martina, M.L.V., Franceschini, S., Pignone, S., Simoni, A., and Pizziolo, M.:  
26 Probabilistic rainfall thresholds for landslide occurrence using a Bayesian approach, *J.*  
27 *Geophys. Res.-Earth*, 117, F04006, doi: 10.1029/2012JF002367, 2012
- 28 Bonaccorso, B., Cancelliere, A., and Rossi, G.: Detecting trends of extreme rainfall series in  
29 Sicily, *Advances in Geosciences*, 2, 7-11, doi: 10.5194/adgeo-2-7-2005, 2005

- 1 Brunetti, M.T., Peruccacci, S., Rossi, M., Luciani, S., Valigi, D., and Guzzetti, F.: Rainfall  
2 thresholds for the possible occurrence of landslides, *Nat. Hazard. Earth Sys.*, 10, 447-458,  
3 doi: 10.5194/nhess-10-447-2010, 2010
- 4 Caine, N.: The rainfall intensity-duration control of shallow landslides and debris flows,  
5 *Geogr. Ann. A*, 62, 23–27, doi: 10.2307/520449, 1980
- 6 Catalano, S., and De Guidi, G.: Late Quaternary uplift of northeastern Sicily: relation with the  
7 active normal faulting deformation, *J. Geodyn.*, 36, 445-467, doi: 10.1016/S0264-  
8 3707(02)00035-2, 2003
- 9 Cuppari, P.: Del quadruplice temporale di Messina. Breve cenno, letto dal Prof. Antonio  
10 Cuppari nell'Adunanza ordinaria del 1° Marzo 1856, *Atti della Reale Accademia dei*  
11 *Georgofili di Firenze*, 3, 171-187, 1856
- 12 Del Ventisette, C., Garfagnoli, F., Ciampalini, A., Battistini, A., Gigli, G., Moretti, S., and  
13 Casagli, N.: An integrated approach to the study of catastrophic debris-flows: geological  
14 hazard and human influence, *Nat. Hazard. Earth Sys.*, 12, 2907-2922, doi: 10.5194/nhess-12-  
15 2907-2012, 2012
- 16 Di Stefano, E., Agate, A., Incarbona, A., Russo, F., Sprovieri, R., and Bonomo, S.: Late  
17 Quaternary high uplift rates in northeastern Sicily: evidence from calcareous nannofossils and  
18 benthic and planktonic foraminifera, *Facies*, 58, 1–15, doi: 10.1007/s10347-011-0271-3, 2012
- 19 Ehret, U.: Rainfall and flood nowcasting in small catchments using weather radar, PhD thesis,  
20 University of Stuttgart, Germany, 262 pp., 2002
- 21 Frattini, P., Crosta, G., and Sosio, R.: Approaches for defining thresholds and return periods  
22 for rainfall-triggered shallow landslides, *Hydrol. Process.*, 23, 1444-1460, doi:  
23 10.1002/hyp.7269, 2009
- 24 Gardner, W.R.: Some steady-state solutions of the unsaturated moisture flow equation with  
25 application to evaporation from a water table, *Soil Sci.*, 85, 228-232, doi: 0.1097/00010694-  
26 195804000-00006, 1958
- 27 Ghezzehei, T.A., Kneafsey, T.J., and Su, G.W.: Correspondence of the Gardner and van  
28 Genuchten-Mualem relative permeability function parameters, *Water Resour. Res.*, 43,  
29 W10417, doi: 10.1029/2006WR005339, 2007

1 Glade, T.: Establishing the frequency and magnitude of landslide-triggering rainstorm events  
2 in New Zealand, *Environ. Geol.*, 35, 160-174, doi: 10.1007/s002540050302, 1997

3 Greenwood, J.A., Landwehr, J.M., Matalas, N.C., and Wallis, J.R.: Probability weighted  
4 moments: definition and relation to parameters of several distribution expressible in inverse  
5 form, *Water Resour. Res.*, 15, 1049-1054, doi: 10.1029/WR015i005p01049, 1979

6 Grelle, G., Soriano, M., Revellino, P., Guerriero, L., Anderson, M.G., Diambra, A., Fiorillo,  
7 F., Esposito, L., Diodato, N., and Guadagno, F.M.: Space-time prediction of rainfall-induced  
8 shallow landslides through a combined probabilistic/deterministic approach, optimized for  
9 initial water table conditions, *B. Eng. Geol. Environ.*, 73, 877-890, doi: 10.1007/s10064-013-  
10 0546-8, 2014

11 Guzzetti, F., Peruccacci, S., Rossi, M., and Stark, C.P.: Rainfall thresholds for the initiation of  
12 landslides in central and southern Europe, *Meteorol. Atmos. Phys.*, 98, 239-267, doi:  
13 10.1007/s00703-007-0262-7, 2007

14 Guzzetti, F., Peruccacci, S., Rossi, M., and Stark, C.P.: The rainfall intensity-duration control  
15 of shallow landslides and debris flows: an update, *Landslides*, 5, 3-17, doi: 10.1007/s10346-  
16 007-0112-1, 2008

17 Hawke, R., and McConchie, J.: In situ measurement of soil moisture and pore-water pressures  
18 in an 'incipient' landslide: Lake Tutira, New Zealand, *J. Environ. Manage.*, 92, 266-274, doi:  
19 10.1016/j.jenvman.2009.05.035, 2011

20 Hosking, J.R.M., Wallis, J.R., and Wood, E.F.: Estimation of the generalized extreme value  
21 distribution by the method of probability weighted moments, *Technometrics*, 27, 251-261,  
22 doi: 10.1080/00401706.1985.10488049, 1985

23 Houghton, J.T., Ding, Y., Griggs, D.J., Noguers, M., van der Linden, P.J., Dai, X., Maskell,  
24 K., and Johnson, C.A.: *Climate Change 2001: The Scientific Basis. Contribution of Working  
25 Group I to the Third Assessment Report of the Intergovernmental Panel on Climate Change*,  
26 Cambridge University Press, Cambridge, UK/New York, USA, 881 pp., 2001

27 Hungr, O., Leroueil, S., and Picarelli, L.: The Varnes classification of landslide types, an  
28 update, *Landslides*, 11, 167-194, doi: 10.1007/s10346-013-0436-y, 2014

29 Iovine, G., Di Gregorio, S., and Lupiano, V.: Debris-flow susceptibility assessment through  
30 cellular automata modeling: an example from 15–16 December 1999 disaster at Cervinara and

1 San Martino Valle Caudina (Campania, southern Italy), *Nat. Hazard. Earth Sys.*, 3, 457–468,  
2 doi: 10.5194/nhess-3-457-2003, 2003

3 Iverson, R.M.: Landslide triggering by rain infiltration, *Water Resour. Res.*, 36, 1897-1910,  
4 doi: 10.1029/2000WR900090, 2000

5 Jacob, M., and Hungr, O.: *Debris-flow Hazards and Related Phenomena*, Springer-Praxis  
6 Publishing Ltd, Chichester, UK, 739 pp., 2005

7 Jenkinson, A.F: The frequency distribution of the annual maximum (or minimum) values of  
8 meteorological events, *Q. J. Roy. Meteor. Soc.*, 87, 158-171, doi: 10.1002/qj.49708134804,  
9 1955

10 Jensen, D.T., Hargreaves, G.H., Temesgen, B., and Allen, R.G.: Computation of ETo under  
11 nonideal conditions, *J. Irrig. Drain. E-Asce*, 123, 394-400, doi: 10.1061/(ASCE)0733-  
12 9437(1997)123:5(394), 1997

13 Johnson, A.I.: *Specific yield-compilation of specific yields for various materials*, U.S.  
14 Geological Survey, Water Supply Paper, 1662-D, 74 pp., 1967

15 Lentini, F., Catalano, S., and Carbone, S.: *Note illustrative della carta geologica della*  
16 *Provincia di Messina scala 1:50.000 S.EL.CA.*, Florence, Italy, 19 pp., 2000

17 Lo, W.C., Lin, B.S., Ho, H.C., Keck, J., Yin, H.Y., and Shan, H.Y.: A simple and feasible  
18 process for using multi-stage high-precision DTMs, field surveys and rainfall data to study  
19 debris flow occurrence factors of Shenmu area, Taiwan, *Nat. Hazard. Earth Sys.*, 12, 3407–  
20 3419, doi: 10.5194/nhess-12-3407-2012, 2012

21 Loheide II, S.P., Butler Jr, J.J., and Gorelick, S.M.: Estimation of groundwater consumption  
22 by phreatophytes using diurnal water table fluctuations: a saturated-unsaturated flow  
23 assessment, *Water Resour. Res.*, 41, W07030, doi: 10.1029/2005WR003942, 2005

24 Lu, N., and Godt, J.W.: Infinite-slope stability under steady unsaturated conditions, *Water*  
25 *Resour. Res.*, 44, W11404, doi: 10.1029/2008WR006976, 2008

26 Lu, N., Godt, J.W., and Wu, D.T.: A closed-form equation for effective stress in unsaturated  
27 soil, *Water Resour. Res.*, 46, W05515, doi: 10.1029/2009WR008646, 2010

28 Mair, A., and Fares, A.: Comparison of rainfall interpolation methods in a mountainous  
29 region of a tropical island, *J. Hydrol. Eng.*, 16, 371-383, doi: 10.1061/(ASCE)HE.1943-  
30 5584.0000330, 2011



1 Melfi, D., Zauli, F., Biron, D., Vocino, A., and Sist, M.: The impact of NEFODINA  
2 convective clouds identification in the rain rate retrieval of H-SAF, in: Proceedings of the  
3 2012 EUMETSAT Meteorological Satellite Conference, Sopot, Poland, September 3<sup>rd</sup> – 7<sup>th</sup>,  
4 2012, 2012

5 Montgomery, D.R., and Dietrich, W.E.: A physically based model for the topographic control  
6 on shallow landsliding, *Water Resour. Res.*, 30, 1153–1171, doi: 10.1029/93WR02979, 1994

7 Mugnai, A., Casella, D., Cattani, E., Dietrich, S., Laviola, S., Levizzani, V., Panegrossi, G.,  
8 Petracca, M., Sanò, P., Di Paola, F., Biron, D., De Leonibus, L., Melfi, D., Rosci, P., Vocino,  
9 A., Zauli, F., Pagliara, P., Puca, S., Rinollo, A., Milani, L., Porcù, F., and Gattari, F.:  
10 Precipitation products from the hydrology SAF, *Nat. Hazard. Earth Syst*, 13, 1959-1981, doi:  
11 10.5194/nhess-13-1959-2013, 2013

12 Nadim, F., Kjekstad, O., Peduzzi, P., Herold, C., and Jaedicke, C.: Global landslide and  
13 avalanche hotspots, *Landslides*, 3, 159-173, doi: 10.1007/s10346-006-0036-1, 2006

14 Nimmo, J.R.: Unsaturated zone flow processes, in: *Encyclopedia of Hydrological Sciences:*  
15 *part 13 Groundwater*, Anderson, M.G. and Bear, J. (Eds.), Wiley, Chichester, UK, 2299-2322,  
16 2005

17 Pegram, G.: Spatial interpolation and mapping of rainfall (SIMAR) – Volume 3: Data  
18 merging for rainfall map production, Water Resource Commission Report n. 1153/1/04, 2003

19 Penna, D., Borga, M., Aronica, G.T., Brigandì, G., and Tarolli, P.: The influence of grid  
20 resolution on the prediction of natural and road-related shallow landslides, *Hydrol. Earth Syst.*  
21 *Sc.*, 18, 2127-2139, doi: 10.5194/hess-18-2127-2014, 2014

22 Peres, D.J., and Cancelliere, A.: Derivation and evaluation of landslide triggering thresholds  
23 by a Monte Carlo approach, *Hydrol. Earth Syst. Sc.*, 18: 4913-4931, doi:10.5194/hess-18-  
24 4913-2014, 2014

25 Petley, D.N.: Global patterns of loss of life from landslides, *Geology*, 40, 927-930, doi:  
26 10.1130/G33217.1, 2012

27 Ray, R.L., and Jacobs, J.M.: Relationships among remotely soil moisture, precipitation and  
28 landslide events, *Nat. Hazards*, 43, 211-222, doi: 10.1007/s11069-006-9095-9, 2007

1 Ray, R.L., Jacobs, J.M., and Cosh, M.H.: Landslide susceptibility mapping using downscaled  
2 AMSR-E soil moisture: A case study from Cleveland Corral, California, US, *Remote Sens.*  
3 *Environ.*, 114, 2624-2636, doi: 10.1016/j.rse.2010.05.033, 2010

4 Reichenbach, P., Cardinali, M., De Vita, P., and Guzzetti, F.: Regional hydrological  
5 thresholds for landslides and floods in the Tiber River Basin (central Italy), *Environ. Geol.*,  
6 35, 146-159, doi: 10.1007/s002540050301, 1998

7 Salciarini, D., Godt, J.W., Savage, W.Z., Conversini, P., and Baum, R.L.: Modeling regional  
8 initiation of rainfall-induced shallow landslides in the eastern Umbria Region of central Italy,  
9 *Landslides*, 3, 181-194, doi: 10.1007/s10346-006-0037-0, 2006

10 Saulnier, G.M., Beven, K., and Obled, C.: Including spatially variable effective soil depths in  
11 TOPMODEL, *J. Hydrol.*, 202, 158–172, doi: 10.1016/S0022-1694(97)00059-0, 1997

12 Savage, W.Z., Godt, J.W., and Baum, R.L.: A model for spatially and temporally distributed  
13 shallow landslide initiation by rainfall infiltration, in: *Debris-Flow Hazards Mitigation:*  
14 *Mechanics, Prediction and Assessment*, Rickenmann, D. and Chen, C.L. (Eds.), Millpress,  
15 Rotterdam, 179-187, 2003

16 Schaap, M.G., Leij, F.J., and van Genuchten, M.Th.: ROSETTA: a computer program for  
17 estimating soil hydraulic parameters with hierarchical pedotransfer functions, *J. Hydrol.*, 251,  
18 163-176, doi: 10.1016/S0022-1694(01)00466-8, 2001

19 Schilirò, L., and Esposito, C.: Susceptibility assessment and triggering scenarios for shallow  
20 landslides in the southern Messina province (north-eastern Sicily, Italy) using statistic-  
21 probabilistic and deterministic approaches, *Rendiconti online della Società Geologica*  
22 *Italiana*, 24, 298-300, 2013

23 Schilirò, L., De Blasio, F.V., Esposito, C., and Scarascia Mugnozza, G.: Reconstruction of a  
24 destructive debris-flow event via numerical modeling: the role of valley geometry on flow  
25 dynamics, *Earth Surf. Processes*, in press, doi: 10.1002/esp.3762, 2015

26 Serrano, S.E.: *Hydrology for Engineers, Geologists, and Environmental Professionals: An*  
27 *Integrated Treatment of Surface, Subsurface, and Contaminant Hydrology*, Second Edition,  
28 Hydroscience Inc., USA, 590 pp., 2010

29 Šimůnek, J., Huang, M., Šejna, M., and van Genuchten, M.Th.: The HYDRUS-1D software  
30 package for simulating the one-dimensional movement of water, heat, and multiple solutes in

1 variably-saturated media. Version 1.0, International Ground Water Modeling Center,  
2 Colorado School of Mines, Golden, Colorado, 186 pp., 1998

3 Terlien, M.T.J.: The determination of statistical and deterministic hydrological landslide-  
4 triggering thresholds, *Environ. Geol.*, 35, 124-130, doi: 10.1007/s002540050299, 1998

5 Trigila, A., Iadanza, C., Esposito, C., and Scarascia Mugnozza, G.: Comparison of Logistic  
6 Regression and Random Forests techniques for shallow landslide susceptibility assessment in  
7 Giampileri (NE Sicily, Italy), *Geomorphology*, in press, doi:  
8 10.1016/j.geomorph.2015.06.001, 2015

9 van Genuchten, M.Th.: A closed-form equation for predicting the hydraulic conductivity of  
10 unsaturated soils, *Soil Sci. Soc. Am. J.*, 44, 892-898, doi:  
11 10.2136/sssaj1980.03615995004400050002x, 1980

12 Vanapalli, S.K., and Fredlund, D.G.: Comparison of different procedures to predict  
13 unsaturated soil shear strength, in: *Advances in Unsaturated Geotechnics*, Shackelford, C.D.,  
14 Houston, S.L., and Chang, N.Y. (Eds.), Society of Civil Engineers, 2000

15 Warrick, A.W.: Correspondence of hydraulic functions for unsaturated soils, *Soil Sci. Soc.*  
16 *Am. J.*, 59, 292–299, doi: 10.2136/sssaj1995.03615995005900020003x, 1995

17 Wieczorek, G.F., and Glade, T.: Climatic factors influencing occurrence of debris flows, in:  
18 *Debris-flow Hazards and Related Phenomena*, Jacob, M. and Hungr, O. (Eds.), Springer-  
19 Praxis Publishing Ltd, Chichester, UK, 325-362, 2005

20 Wilson, R.C., and Wieczorek, G.F.: Rainfall thresholds for the initiation of debris flow at La  
21 Honda, California, *Environ. Eng. Geosci.*, 1, 11–27, 1995

22

1 Table 1. Physical and mechanical properties of the colluvial deposit.

<i>Physical properties</i>			
Unit weight of soil solids (kN m <sup>-3</sup> )	26.73		
Porosity (%)	35		
<i>Granulometric characteristics</i>			
n. sample	1	2	3
Gravel (%)	58.1	53.9	24.2
Sand (%)	34.9	27.0	52.5
Silt (%)	5.9	14.8	15.3
Clay (%)	1.1	4.4	8.0
<i>Mechanical properties</i>			
Friction angle (°)	30-40		
Cohesion (kN m <sup>-2</sup> )	0-5		

2

1 Table 2. Resulting average volumetric-gravimetric water content ( $\theta$  and  $w$ , respectively) and  
2 degree of saturation ( $S_r$ ) at four different simulation times (1, 24, 25 and 30 September).

<i>Date (day-month)</i>	$\theta$ (-)	$w$ (%)	$S_r$ (%)
01-Sept.	0.047	2.65	13.4
24-Sept.	0.182	10.3	52.1
25-Sept.	0.194	11.0	55.4
30-Sept.	0.19	10.8	54.4

3

1 Table 3. Input parameters for TRIGRS model.

<i>Parameter</i>		<i>Attributed value</i>	<i>Source</i>
H (m)	Soil thickness	Spatial map	Saulnier et al., 1997
$I_z$ ( $m s^{-1}$ )	Rainfall rate	Spatial-temporal maps	Ehret, 2002; Pegram, 2003
$\phi'$ ( $^\circ$ )	Friction angle	35	Lab tests + references
$c'$ ( $kN m^{-2}$ )	Cohesion	3	Lab tests + references
$\gamma_n$ ( $kN m^{-3}$ )	Soil unit weight	19.22	Lab tests + HYDRUS 1-D
$\theta_s$ (-)	Saturated water content	0.3831	HYDRUS 1-D
$\theta_r$ (-)	Residual water content	0.046	HYDRUS 1-D
$K_s$ ( $m s^{-1}$ )	Saturated hydraulic conductivity	$6.6 \times 10^{-5}$	HYDRUS 1-D
$d_{wt}$ (m)	Initial water table depth	H	HYDRUS 1-D
$\alpha_G$ ( $m^{-1}$ )	Gardner parameter	11.8	HYDRUS 1-D + Ghezzehei et al., 2007
$I_{ZLT}$ ( $m s^{-1}$ )	Background rainfall rate	$8.49 \times 10^{-8}$	HYDRUS 1-D
$D_0$ ( $m^2 s^{-1}$ )	Hydraulic diffusivity	$1.55 \times 10^{-4}$	Johnson, 1967; Grelle et al., 2014

2

1 Table 4. Results of TRIGRS simulation at different times: number and relative percentage of  
 2 pixels predicted as unstable ( $P_U$ ); percentage of correctly predicted landslide ( $P_L$ ) and stable  
 3 ( $P_S$ ) pixels.

<i>Time</i>	<i>n. unstable pixels</i>	<i><math>P_U</math> (%)</i>	<i><math>P_L</math> (%)</i>	<i><math>P_S</math> (%)</i>
13:00 UTC	260	0.2	0.03	99.95
14:00 UTC	432	0.3	0.1	99.93
15:00 UTC	1,359	1.1	0.54	99.72
16:00 UTC	6,579	5.2	3.46	98.70
17:00 UTC	23,203	18.4	14.79	95.48
18:00 UTC	49,950	39.6	30.26	90.22
19:00 UTC	71,473	56.6	42.44	85.98
20:00 UTC	108,222	85.7	61.38	78.68
21:00 UTC	126,207	100	68.81	75.05

4

1 Table 5. Parameters derived from HYDRUS 1-D simulations, considering the grain size  
 2 characteristics of the three soil samples.

<i>Parameter</i>		<i>Sample n.1</i>	<i>Sample n.2</i>	<i>Sample n.3</i>
$\theta_s$ (-)	Saturated water content	0.3831	0.3872	0.3837
$\theta_r$ (-)	Residual water content	0.046	0.039	0.042
$K_s$ (m s <sup>-1</sup> )	Saturated hydraulic conductivity	$6.6 \times 10^{-5}$	$1.25 \times 10^{-5}$	$7.91 \times 10^{-6}$
$\alpha_G$ (m <sup>-1</sup> )	Gardner parameter	11.8	11.1	12.2
$I_{ZLT}$ (m s <sup>-1</sup> )	Background rainfall rate	$8.49 \times 10^{-8}$	$5.35 \times 10^{-8}$	$5.37 \times 10^{-8}$
$D_0$ (m <sup>2</sup> s <sup>-1</sup> )	Hydraulic diffusivity	$1.55 \times 10^{-4}$	$3.84 \times 10^{-5}$	$2.43 \times 10^{-5}$

3



1 Table 6. Estimated return period (RP) in years for rainfall accumulated in the 1, 2, 5, 10, 20,  
2 30, 60, 90, 120 and 180 days prior to 1 October 2009 for Santo Stefano di Briga (SSB) and  
3 Messina Istituto Geofisico (MIG) rainfall stations.

<i>Cumulated days</i>	<i>RP (SSB)</i>	<i>RP (MIG)</i>
1	47	4
2	22	2
5	8	1
10	12	5
20	7	4
30	4	2
60	1	1
90	1	1
120	1	1
180	1	1

4

1 Table 7. Estimated return period (RP) in years for rainfall accumulated in 1, 3, 6, 12 and 24  
2 hours during the 1 October 2009 event.

<i>Cumulated hours</i>	<i>RP</i>
1	78
3	26
6	40
12	39
24	19

3

1 Table 8. Number of unstable pixels predicted by TRIGRS at the end of the simulated rainfall  
 2 scenario T(0) and in the next two hours T(1h) and T(2h).  $P_{2009}$  represents the percentage of  
 3 the maximum number of predicted unstable pixels compared to those obtained in the back-  
 4 analysis of the 1 October 2009 event.

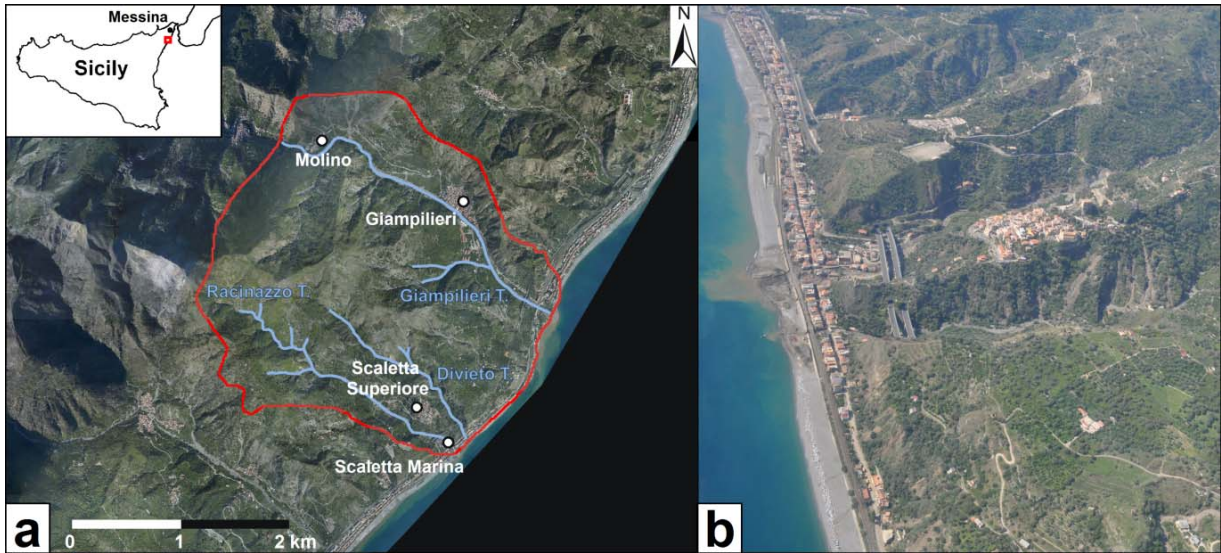
<i>Rainfall duration</i>	<i>RP (year)</i>	<i>Rainfall amount (mm)</i>	<i>Rainfall rate (mm/h)</i>	<i>n. unstable pixels</i>			<i>P<sub>2009</sub> (%)</i>
				<i>T (0)</i>	<i>T (1h)</i>	<i>T (2h)</i>	
1 hour	2	30	30	11,605	23,123	21,513	18.3
	4	45	45	20,154	38,127	36,904	30.2
	10	55	55	24,643	47,790	47,729	37.9
	20	65	65	28,578	57,530	56,762	45.6
3 hours	2	45	15	8,069	8,103	6,623	6.4
	4	60	20	29,632	34,464	32,448	27.3
	10	85	28.3	51,268	61,745	59,361	48.9
	20	105	35	65,558	82,398	79,865	65.3
6 hours	2	55	9.2	5,387	4,608	4,446	4.3
	4	70	11.7	5,641	4,654	4,451	4.5
	10	95	15.8	35,671	36,053	34,091	28.6
	20	120	20	63,992	68,697	65,910	54.4
12 hours	2	60	5	4,983	4,494	4,419	3.9
	4	85	7.1	5,187	4,528	4,425	4.1
	10	110	9.2	5,387	4,571	4,429	4.3
	20	130	10.8	5,552	4,602	4,436	4.4

5

1 Table 9. Number of unstable pixels predicted by TRIGRS by using the rainfall amounts  
 2 recorded during the 25 October 2007 and 1 October 2009 event. Data have been computed at  
 3 the end of the simulated rainfall scenario T(0) and in the next two hours T(1h) and T(2h).  
 4 P<sub>2009</sub> represents the percentage of the maximum number of predicted unstable pixels  
 5 compared to those obtained in the back-analysis of the 1 October 2009 event.

<i>Rainfall duration</i>	<i>RP (year)</i>	<i>Rainfall amount (mm)</i>	<i>Rainfall rate (mm/h)</i>	<i>n. unstable pixels</i>			<i>P<sub>2009</sub> (%)</i>
				<i>T (0)</i>	<i>T (1h)</i>	<i>T (2h)</i>	
1 hour	20 (2007)	65	65	28,578	57,530	56,762	45.6
	78 (2009)	85	85	35,041	78,291	75,913	62.0
3 hours	26 (2009)	115	38.3	72,493	92,322	90,391	73.2
	30 (2007)	120	40	85,348	106,568	104,704	84.4
6 hours	28 (2007)	130	21.7	83,704	92,944	90,532	73.6
	40 (2009)	142	23.7	85,777	93,831	90,952	74.3
12 hours	20 (2007)	130	10.8	5,552	4,602	4,436	4.4
	39 (2009)	153	12.7	9,377	6,938	6,036	7.4

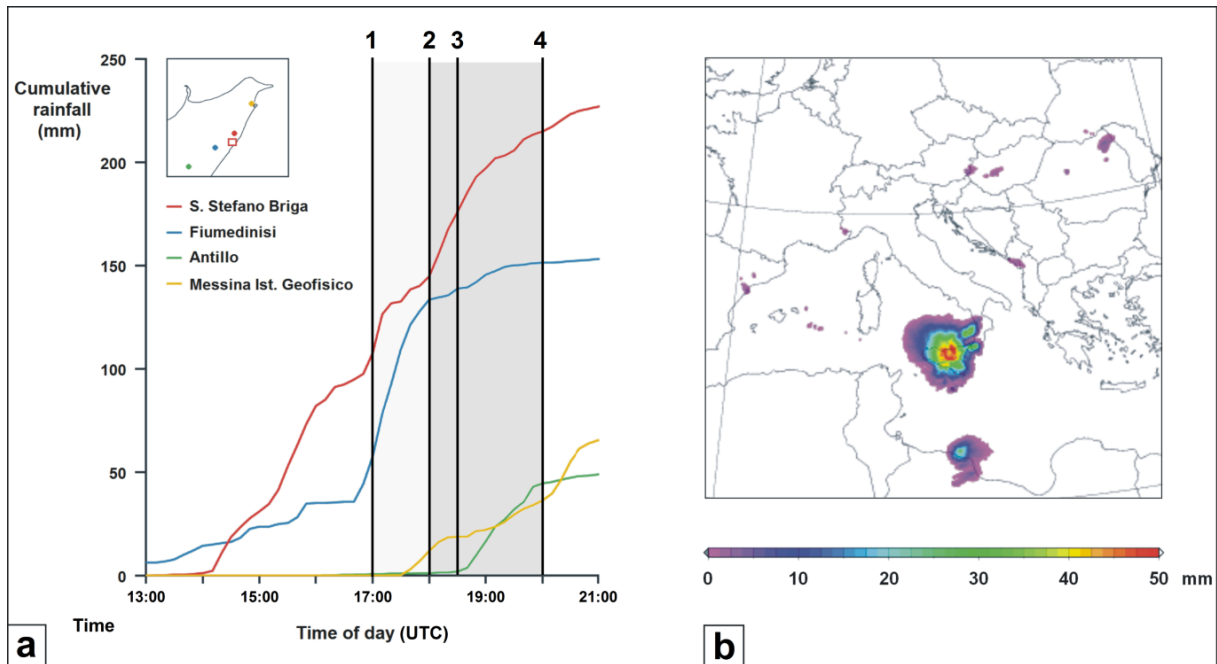
6



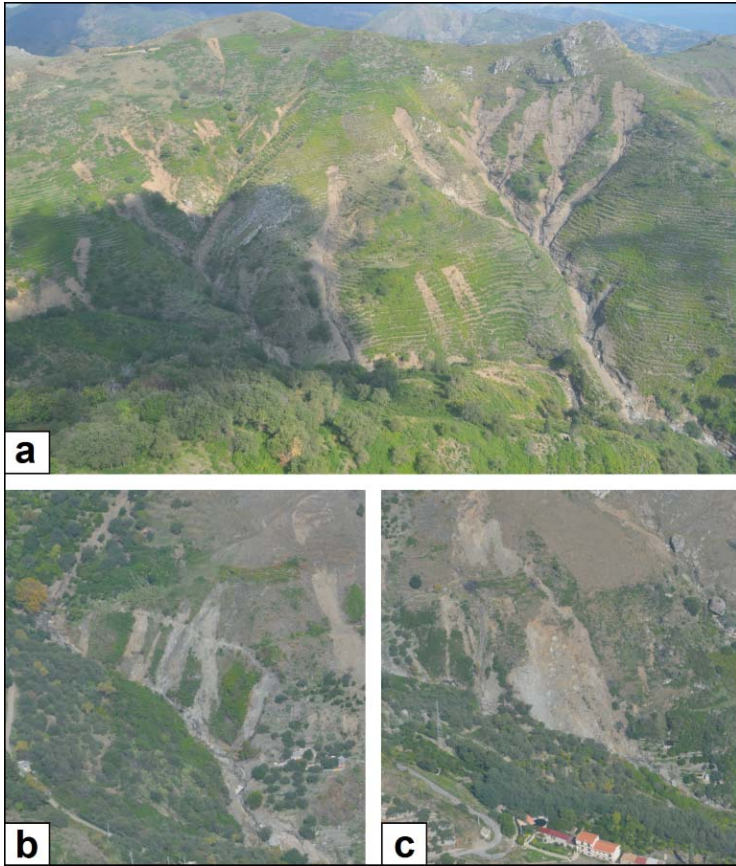
1

2 Figure 1. a) the study area; b) aerial view of Giampileri area a few days after the 1 October  
3 2009 event.

4

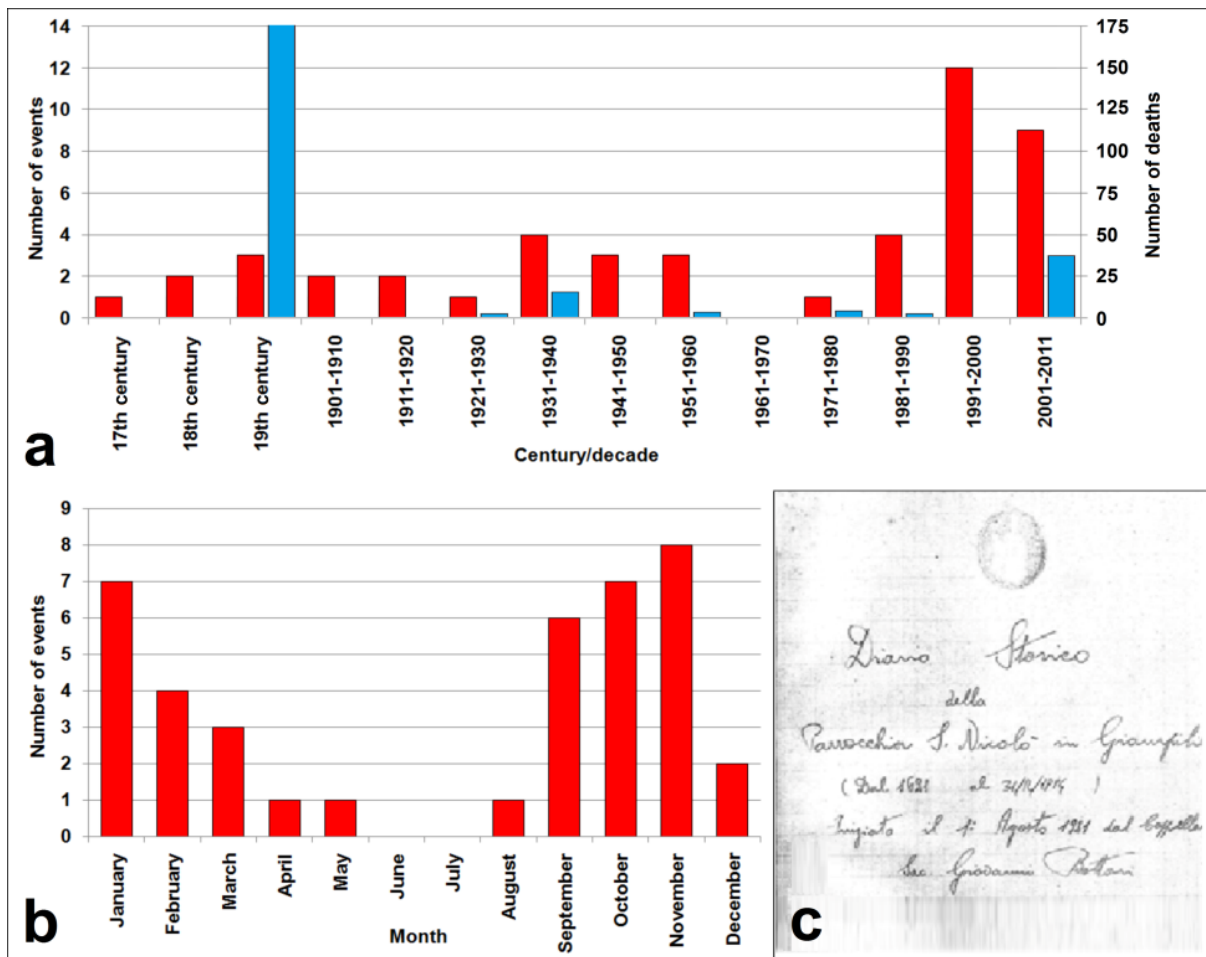


1  
2 Figure 2. a) cumulative hyetographs recorded at the 4 rain gauge stations (Santo Stefano di  
3 Briga, Fiumedinisi, Antillo and Messina Istituto Geofisico), whose location is shown in the  
4 upper left sketch (the red square represents the study area). The shaded areas indicate the  
5 landslide timing during the event, on the basis of witness reports: 1- first landslide events in  
6 Giampilieri village (17:00-17:15 UTC); 2- beginning of the most critical stage, with the  
7 triggering of hundreds of shallow landslides in Giampilieri and the surrounding areas (18:00  
8 UTC); 3- landslides in Molino village (18:30-18:45 UTC); 4- end of the landslide events  
9 (20:00 UTC); b) accumulated rainfall between 18:00 and 21:00 UTC, based on radar  
10 (satellite) data (from Melfi et al., 2012).  
11



1  
2  
3  
4

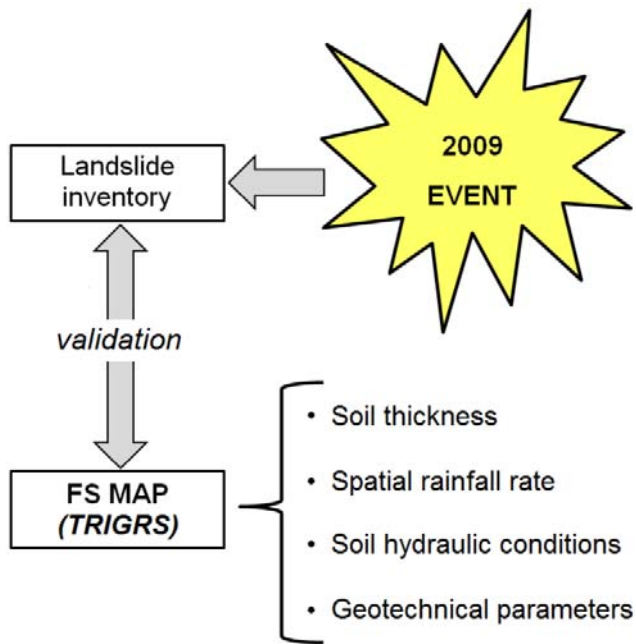
Figure 3. Different types of shallow landslides occurred on 1 October 2009 a) debris-flows; b) debris-slides; c) debris-avalanches.



1  
 2 Figure 4. a) number of landslide/flood events (red bars) and related fatalities (blue bars)  
 3 recorded in the southern Messina area per century/decade; b) number of recorded  
 4 landslide/flood events per month of occurrence; c) frontispiece of the historical diary of S.  
 5 *Nicolò di Giampileri* church.

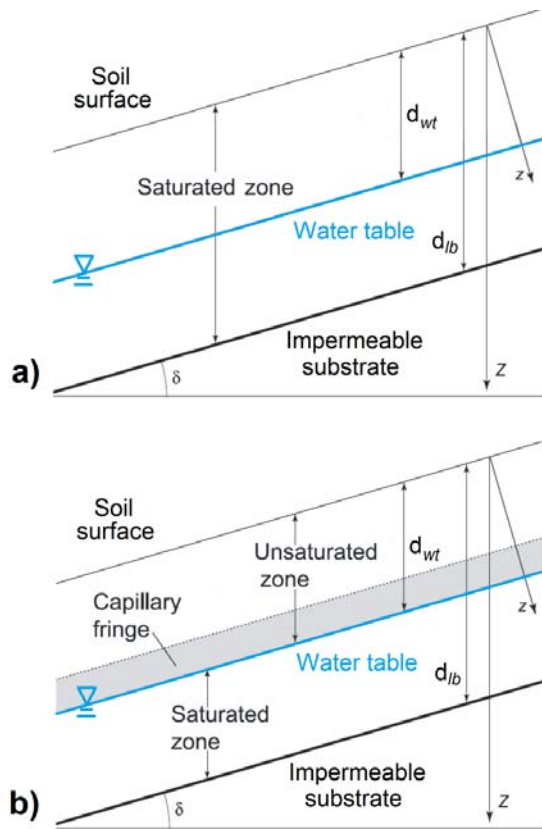
6





1

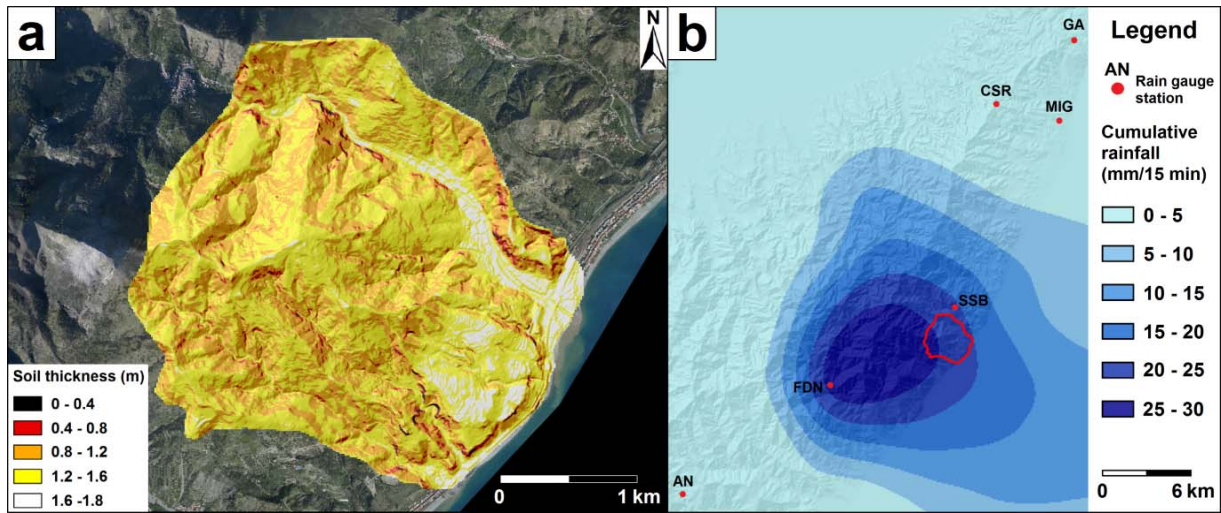
2 Figure 5. Summary of the back-analysis process used for the 2009 event.



1

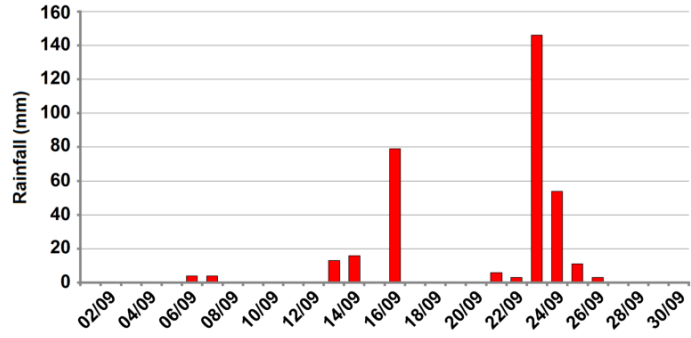
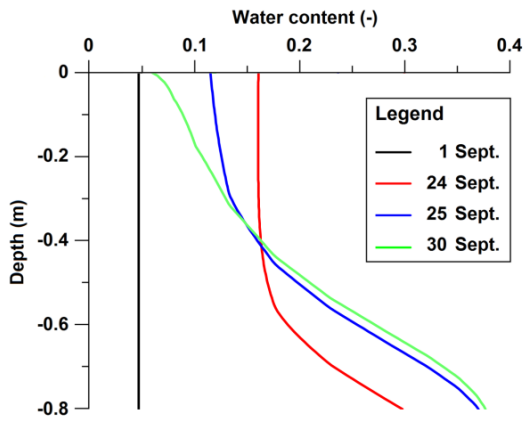
2 Figure 6. Conceptual sketch of the hydrological model in TRIGRS simulating tension-  
 3 saturated (a) and unsaturated (b) soil conditions (from Baum et al., 2010 mod.).

4



1  
 2 Figure 7. a) soil thickness map for the study area; b) an example of rainfall map resulting  
 3 from the application of conditional merging technique: in this case, the cumulative rainfall  
 4 between 17:00 and 17:15 UTC is reported. Points indicate the location of the six rain gauge  
 5 stations used in the method (AN: Antillo, CSR: Colle San Rizzo, FDN: Fiumedinisi, GA:  
 6 Ganzirri, MIG: Messina Istituto Geofisico, SSB: Santo Stefano di Briga).

7



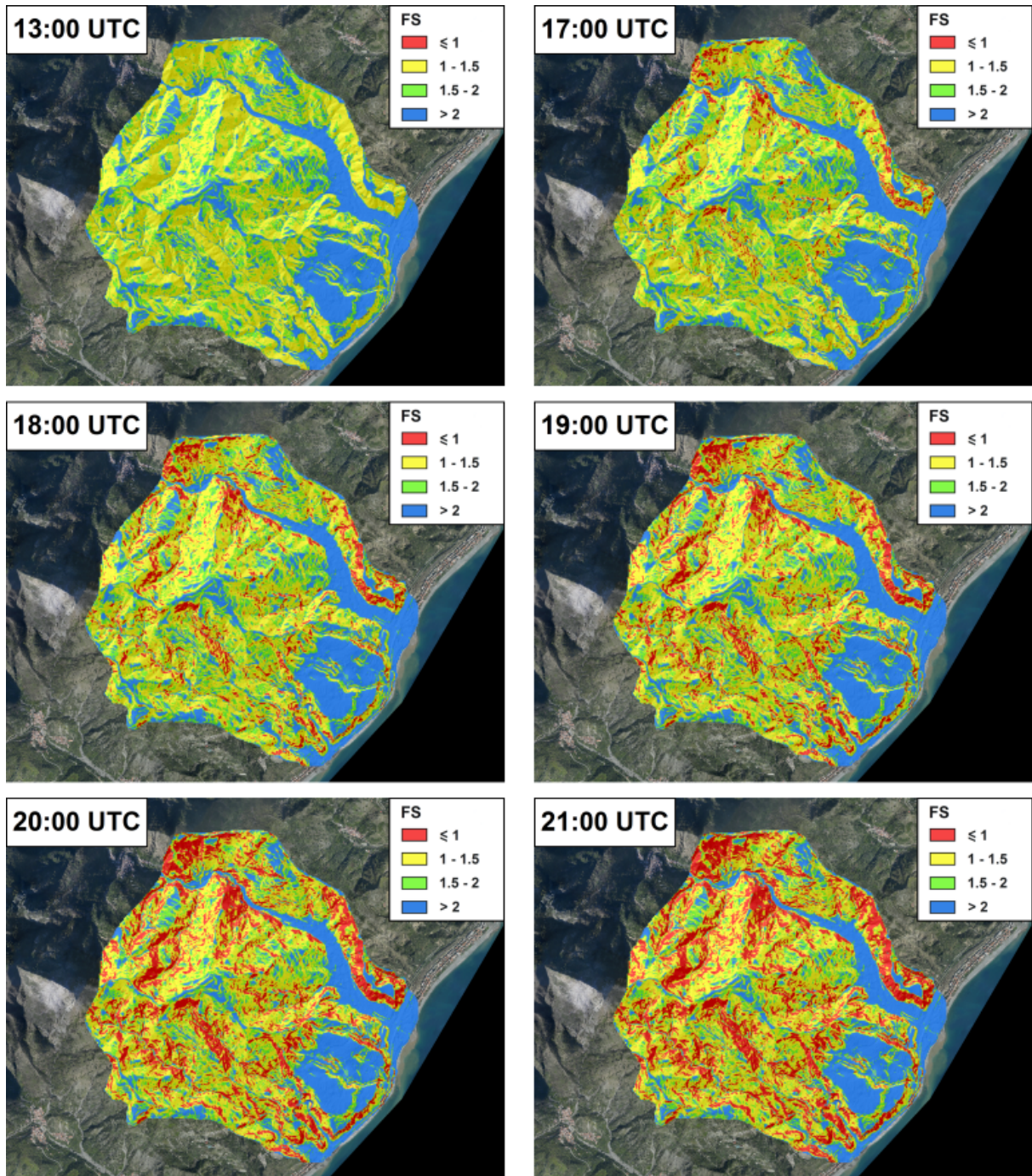
1 **a** **b**

2 Figure 8. a) resulting water content trend vs. depth at four different simulation times (1, 24, 25

3 and 30 September); b) September 2009 daily rainfall data recorded at the Fiumedinisi rain

4 gauge station.

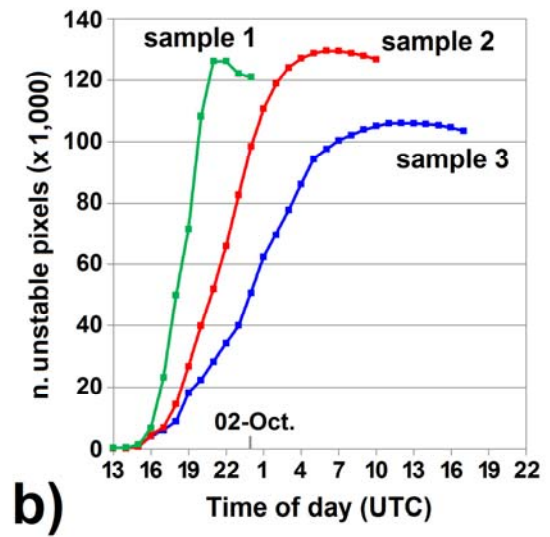
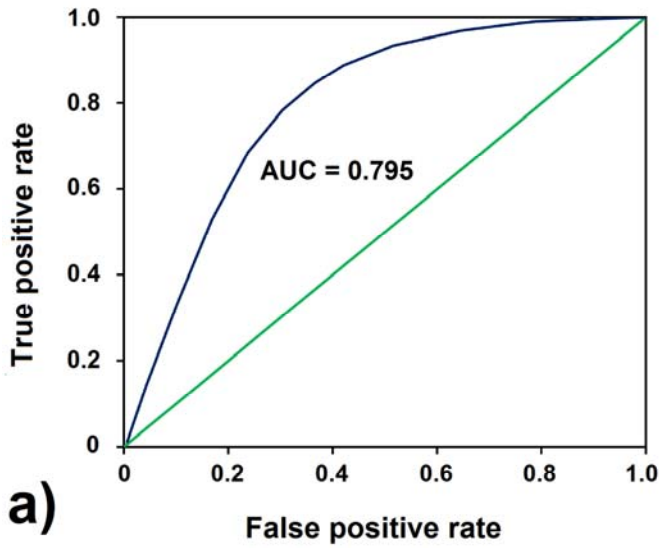
5



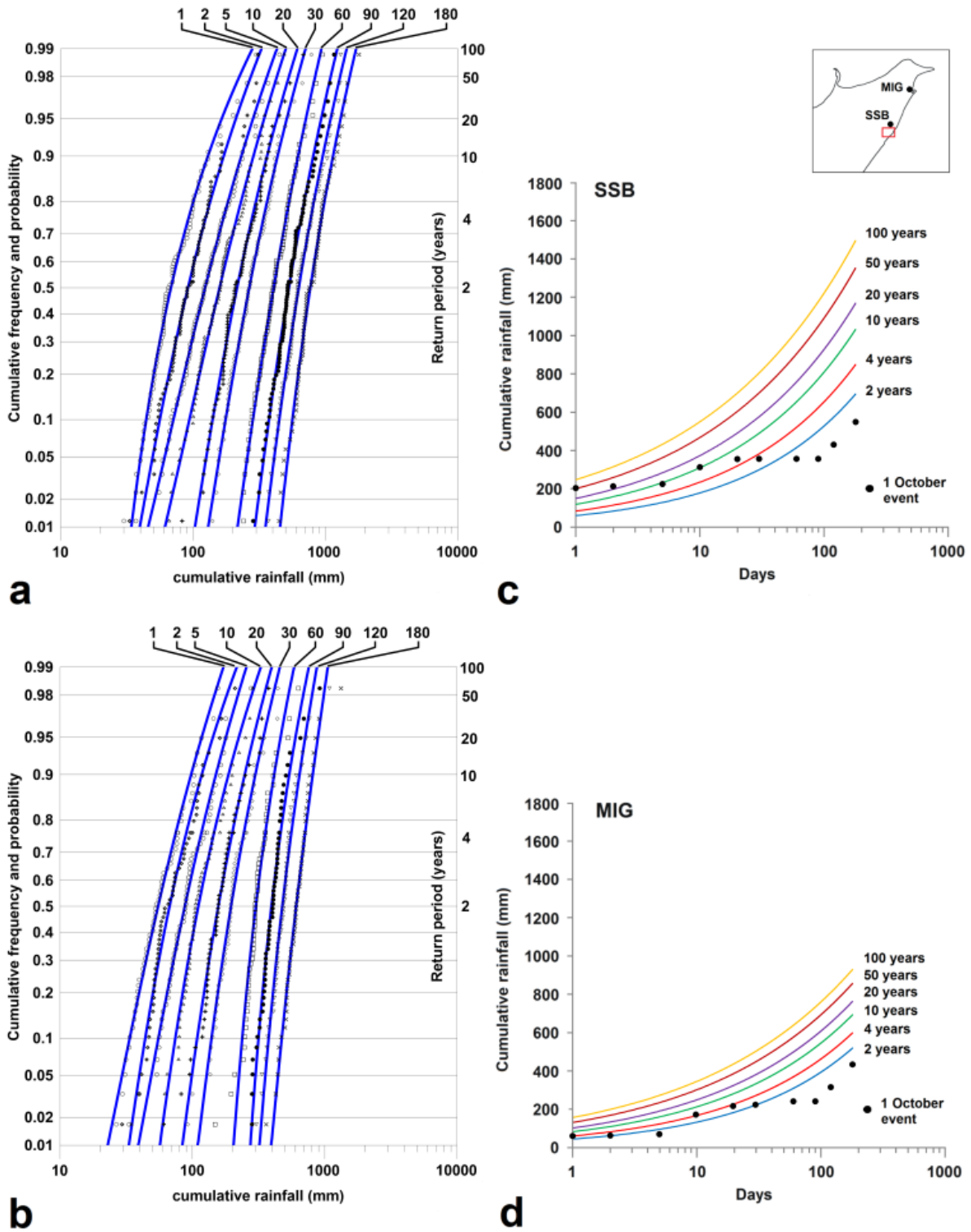
1

2 Figure 9. Slope stability conditions, expressed in terms of safety factor (FS), during the 1  
 3 October 2009 event according to TRIGRS model.

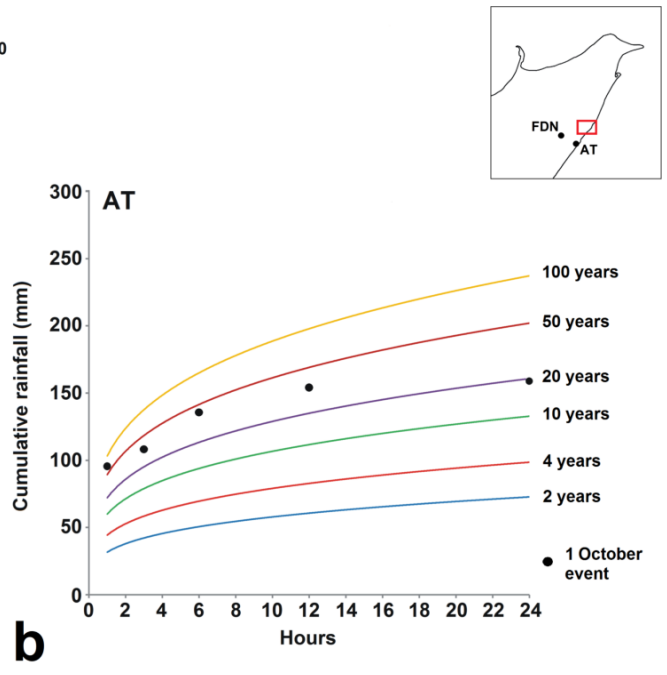
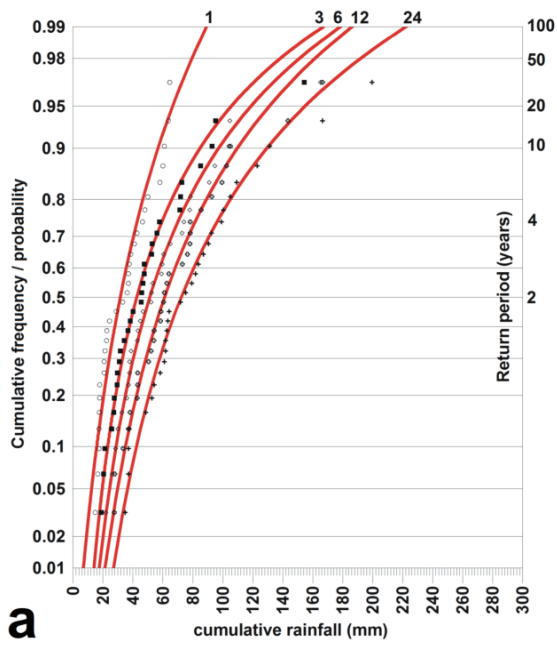
4



1  
 2 Figure 10. a) ROC curve carried out by the comparison between TRIGRS final FS map and 1  
 3 October 2009 landslide inventory map; b) number of unstable pixels computed by TRIGRS  
 4 during the event, considering three different grain size distributions of the investigated soil.  
 5



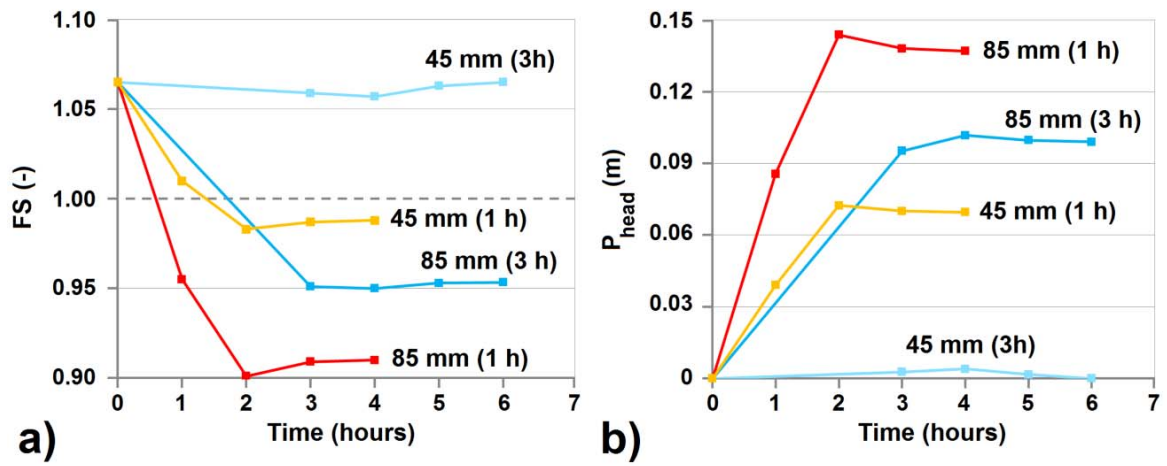
1  
 2 Figure 11. Cumulative frequency and probability according to GEV distribution for 1, 2, 5,  
 3 10, 20, 30, 60, 90, 120 and 180 days cumulative rainfall for (a) Santo Stefano di Briga (SSB)  
 4 and (b) Messina Istituto Geofisico (MIG) station; c-d) rainfall probability curves for return  
 5 periods of 2, 4, 10, 20, 50 and 100 years for the same stations, whose location is shown in the  
 6 upper right sketch (the red square represents the study area).



1  
2  
3  
4  
5  
6  
7

Figure 12. a) cumulative frequency and probability according to GEV distribution for 1, 3, 6, 12 and 24 hours cumulative rainfall for Ali Terme (AT) station; b) rainfall probability curves for return periods of 2, 4, 10, 20, 50 and 100 years for the same station. The location of this station and Fiumedinisi (FDN) one is shown in the upper right sketch (the red square represents the study area).





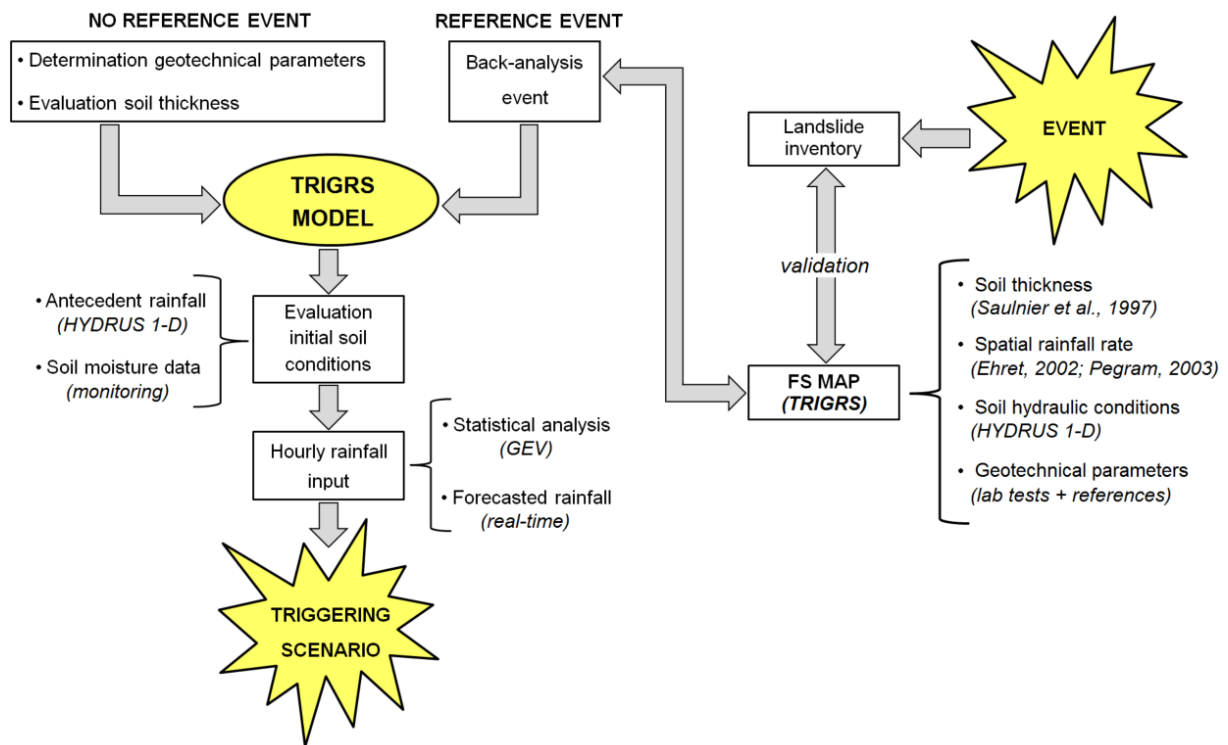
1 **a)**

2 Figure 13. a) Safety Factor (FS) vs. time at the selected grid cell of interest for different

3 rainfall scenarios, based on TRIGRS numerical simulation; b) Pressure head vs. time at the

4 selected grid cell of interest for different rainfall scenarios, based on TRIGRS numerical

5 simulation.



1  
 2 Figure 14. Flux diagram describing the proposed approach for the evaluation of shallow  
 3 landslide triggering scenarios.